24. Sonic Velocities in an Active Gas Hydrate System, Hydrate Ridge[1]

Gilles Guerin,[2] David S. Goldberg,[2] and Tim S. Collett[3]

ABSTRACT

During Ocean Drilling Program Leg 204, sonic logs were recorded in six holes across the southern summit of Hydrate Ridge, to measure in situ the sonic velocities of the sediments in an active gas hydrate system. In addition, vertical seismic profiles were acquired in four of these holes to help the integration of the borehole data within the high-resolution three-dimensional seismic survey of the area. Synthetic seismograms generated from the velocity and the density logs confirm the depth and the nature of the main reflectors identified in the seismic survey. In particular, the bottom-simulating reflector (BSR) was reached in five of the wells and is adequately reproduced by the synthetic seismograms. The most prominent horizons under the crest of Hydrate Ridge, Horizons A, B, and B′, are also reproduced by the synthetics for the wells where they were present. The lower amplitudes of the synthetic reflections suggest that part of the free gas carried by these horizons, which have been identified as conduits to the Hydrate Ridge reservoir, escaped during drilling operation.

We use a model for the cementation of grains by hydrate formation to estimate gas hydrate saturations above the BSR and the Gassmann model with fluid substitution to estimate free gas saturation below the BSR. These elastic models suggest that gas hydrate occupies ~10%–20% of the pore space over the BSR in the holes closest to the crest (Holes 1245E, 1247B, and 1250F) and that gas hydrate saturations further on the flank are <10%. These results agree well overall with saturations derived from resistivity logs by Archie's method but indicate a less heterogeneous gas hydrate distribution than the resistivity logs. The Gassmann model identifies up to 2% of free gas in Horizons A, B, and B′ but also indicates pervasive presence of free gas below the BSR in the

[2]Borehole Research Group, Lamont-Doherty Earth Observatory of Columbia University, Palisades NY 10964, USA. Correspondence author: **guerin@ldeo.columbia.edu**
[3]U.S. Geological Survey, Denver Federal Center, Denver CO 80225, USA.

holes closest to the crest, 1245E, 1247B, and 1250F. In all the holes, the presence of gas hydrate or free gas results in the reduction of sonic logging waveform amplitudes, most prominently the high-frequency dipole waveforms.

INTRODUCTION

As a solid crystalline structure replaces the pore fluid during gas hydrate formation, one of the best recognized indications of the presence of gas hydrate in marine sediments is an increase in the shear and bulk moduli and in sonic velocity. The instability of gas hydrate at surface conditions makes in situ recording of the sediment properties by downhole logging the most accurate way to identify and quantify its distribution. We summarize here the results of the different in situ acoustic measurements made during Ocean Drilling Program (ODP) Leg 204 on Hydrate Ridge, off the coast of Oregon.

After discussing some of the issues associated with processing of the sonic waveforms in such low-velocity formations, we describe the various methods that we use to characterize the acoustic properties of the Hydrate Ridge system. Vertical seismic profiles (VSPs) were collected in four holes to integrate the borehole data with the three-dimensional (3-D) seismic data. We use the direct arrivals derived from the stacked waveforms to calculate interval velocities and to calibrate the time vs. depth (TvD) relationships for correlation between well and seismic data. This correlation is primarily established by generating synthetic seismograms from the density and the compressional velocity (V_P) logs.

Multiple elastic models have been designed to estimate gas hydrate and free gas saturations from acoustic logs (Lee and Collett, 2005; Lee et al., 1996; Helgerud et al., 1999; Murphy, 1984). After comparing some of the most commonly used, Guerin et al. (1999) concluded that the model for cementation of Dvorkin and Nur (1996) was the most appropriate to describe the sediment/hydrate interaction in the Blake Ridge sediments, assuming that gas hydrate is deposited uniformly on the grain surface. We apply this model, assuming also a uniform distribution of gas hydrate on the grain surface, to derive gas hydrate saturations from the Hydrate Ridge sonic and density logs. We use the classic Biot/Gassmann formulation for fluid substitution (Murphy, 1984) to estimate free gas saturations below the bottom-simulating reflector (BSR).

For all the sites, we generate a composite of the different logs associated with the sonic data and the presence of gas hydrate, including the gas hydrate and the free gas saturations derived from wireline logs and the synthetic seismograms generated from the density and V_P logs. The synthetic seismograms are used to identify the correlations between the logs and the high-resolution 3-D seismic survey of the area (Tréhu and Bangs, 2001; Bangs et al., 2005).

The results are presented and discussed site by site, starting from the furthest downdip site on the western flank (Hole 1245E), going updip to the crest sites (Holes 1247B and 1250F), and continuing downdip toward the eastern flank (Hole 1244E) and eastern basin (Holes 1252A and 1251H). We conclude by drawing some of the implications for the Hydrate Ridge gas hydrate system.
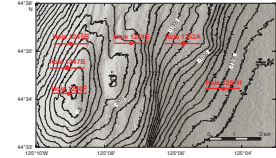
METHODS

Sonic Logs

During ODP Leg 204, sonic logs were recorded with the Schlumberger Dipole Sonic Imager (DSI) in six holes across southern Hydrate Ridge (Fig. F1). One monopole source and two dipole sources were used to generate the V_P and the shear velocity (V_S) logs, respectively. Full waveforms were recorded by the eight-receiver array for each source type. Because of the poorly consolidated nature of the sediments, compressional velocities are very close to the borehole fluid velocity and complete postcruise reprocessing of the monopole waveforms was necessary to discriminate properly the different arrivals and draw accurate V_P logs. Because the DSI was not originally configured for such slow sediments, all the velocity logs were anomalously erratic at the time of the acquisition (see Tréhu, Bohrmann, Rack, Torres, et al., 2003). We used the slowness-time coherence (STC) processing method (Kimball and Marzetta, 1984; Harrison et al., 1990) to reprocess all the waveforms recorded.

In the STC method, a fixed-length window is moved along the first receiver waveform in discrete overlapping time step within a range of possible arrival times. For each time step, the window is moved linearly across the different receivers, the moveout between receivers corresponding to a given velocity, or, more accurately, slowness value. For each time step, the slowness value is then varied in discrete velocity increments within a predefined range. For each time and slowness step, a semblance function is calculated within the time window across the receiver arrays (Kimball and Marzetta, 1984). The peaks in semblance, or in coherence, are assumed to correspond to individual mode arrivals. The method can be refined by constraining accurately the probable arrival times and velocity ranges and by reducing the time and velocity steps. The STC processing routine used was part of the Schlumberger GeoFrame software.

For each hole, we show the results of the STC analysis of all the sonic logging waveforms recorded. The color in these figures represents the projection of the STC plane on the slowness axis. Two logging passes were made in each hole, making it possible to use different source frequencies between passes and thus to investigate the influence of the source frequency on the waveforms in the presence of gas hydrate. The central frequencies used for the monopole source were a "standard" frequency of ~12.5 kHz and a lower frequency of ~6.0 kHz. Unless otherwise indicated on the corresponding figure, the central frequencies of the dipole sources were ~800 Hz for the lower dipole and ~2.0 kHz for the upper dipole. Whereas the amplitude and the character of the recorded waveforms are different depending on the nature and frequency of the acoustic sources, reflecting a possible influence of gas hydrate on the higher frequency waveforms for the dipole, the figures show that, for each hole, the STC results were similar between passes. However, these figures also show that in most cases the lower frequency sources generated a higher coherence across the receiver array and resulted in more robust velocity logs. Consequently, we use only the velocity logs generated with the lower frequency sources in the subsequent analysis of the data, the generation of synthetic seismograms, and the estimation of gas hydrate and free gas saturations.

F1. Map of southern Hydrate Ridge, p. 18.

G. Guerin et al.
Sonic Velocities in an Active Gas Hydrate System

4

Synthetic Seismograms

The generation of synthetic seismograms is a widely recognized method to tie borehole data with seismic surveys (Peterson et al., 1955; Wuenschel, 1960). The V_P and the density (ρ) wireline logs are used to calculate seismic impedance (ρV_P) and generate a reflection coefficient series. The velocity log is integrated into cumulative transit time in order to translate the reflection coefficient series into the time domain. For each hole, a synthetic wavelet was extracted from the 3-D seismic survey by statistical correlations between the seismic traces closest to the borehole location. The synthetic seismogram was then calculated by convolution of the wavelet with the reflection coefficient series. Finally, the resulting synthetic seismograms were tied with the seismic data by identifying the strongest reflectors at the different sites, such as the BSR and Horizons A, B, and B′. We used the IESX seismic integration module of the Schlumberger/GeoQuest GeoFrame software to generate the synthetic seismograms and to integrate the logging data within the 3-D seismic survey.

## Vertical Seismic Profiles

Intermediate in scale and resolution between the sonic logs and the 3-D seismic data, the VSP surveys undertaken during Leg 204 were primarily aimed at defining the gas hydrate distribution on Hydrate Ridge and refining the signature of gas hydrate in the seismic data. They were also used to derive independent TvD relationships that could be used to tie the well data with the seismic data and to calibrate similar relationships derived from the synthetic seismograms. The detail of the operations and a complete description of the tools and methods used is given by Tréhu et al. (this volume).

VSP surveys were attempted at five sites. Because of operational difficulties, only the surveys in Holes 1247B, 1250F, and 1244E were successful in recording coherent waveforms at multiple closely spaced stations. Despite attempts at multiple depths in Hole 1251H, only four stations offered sufficient coupling between the tool and the formation to record clear arrivals. We show the stacked waveforms recorded at all the successful stations in these holes in Figures F2, F3, F4, and F5. The waveforms in these figures have not been corrected for the position of the source and the triggering delay, and the traveltime is not the actual transit time used in the TvD relationship. The sharpness of the first arrivals is an indication of the strength of the coupling between the tool and the formation and consequently of the quality of the data. The correct identification of the first arrivals in Holes 1244E, 1247B, and 1250F allowed us to calculate interval velocity values that could be compared with the V_P logs in these wells. Assuming that the wave path is vertical, the interval velocity between two stations is calculated by dividing the depth span between them by the difference in the first arrival transit times. The resulting velocity is assigned to the middle depth between the two stations. In the figures for the results in Holes 1244E and 1247B, the results have been smoothed by a five-sample moving average window.
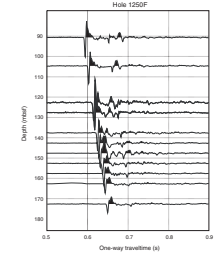
Identification of Gas Hydrate from Elastic Properties

The commonly observed increase in sonic velocity in the presence of gas hydrate can be understood intuitively by the replacement of the
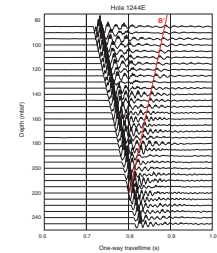
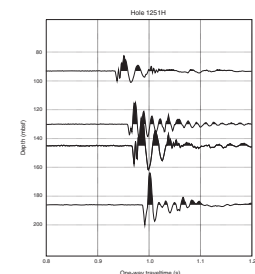F2. Stacked waveforms of the VSP in Hole 1247B, p. 19.
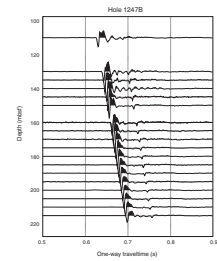
F3. Stacked waveforms of the VSP in Hole 1250F, p. 20.

F4. Stacked waveforms of the VSP in Hole 1244E, p. 21.

F5. Stacked waveforms of the VSP in Hole 1251H, p. 22.

pore fluid by the solid crystalline structure of methane clathrates. However, this simple substitution process is not sufficient to generate the increase in sonic velocity observed, most significantly in shear velocity. Although the purpose of this work is not to compare the merits of the various models existing to estimate gas hydrate saturations from sonic logs, it is necessary to provide an estimate of the gas hydrate saturations that can be associated with the various attributes of the sonic logs discussed.

Guerin et al. (1999) and Guerin and Goldberg (2005) show that some degree of cementation of the sediment grains by gas hydrates must occur to generate the increases in V_P and V_S observed in hydrate-bearing sediments. Guerin et al. (1999) conclude that, among other models, the best description of the elastic properties of the Blake Ridge gas hydrate–bearing sediments is the cementation theory of Dvorkin and Nur (1996), assuming that hydrate is deposited uniformly on the grains. In this formulation, the effect of cementation on the elastic properties is measured by the dry bulk modulus of randomly packed identical grains with interstitial cement (Dvorkin et al., 1994). The dry sediments/hydrate frame is

$$K_{dry} = \frac{n}{6}(1-\phi)\rho_h V_{ph}^2 S_N, \tag{1}$$

where

    n = number of contact points between grains (assumed to be 9),
    ϕ = sediment porosity,
    ρ_h = density, and
    V_{ph} = compressional velocity of gas hydrate (Dvorkin and Nur, 1996).

The normal stiffness S_N is proportional to the stiffness of a cemented two-grains combination. It depends on the amount of cement (i.e., on the gas hydrate saturation S) on the cement/grain configuration and on the elastic properties of gas hydrate and of the grains. A statistical formulation, assuming that gas hydrate is deposited uniformly on the grains, was derived by Dvorkin and Nur (1996):

$$S_N = A_N\alpha^2 + B_N\alpha + C_N, \text{ with} \tag{2}$$

$$A_N = -0.024153\Lambda_N^{-1.3646}, \tag{3a}$$

$$B_N = 0.20405\Lambda_N^{-0.89008}, \tag{3b}$$

$$C_N = 0.00024649\Lambda_N^{-1.9846}, \tag{3c}$$

$$\Lambda_N = \frac{2\mu_h}{\mu_{grain}}\frac{(1-\nu_{grain})(1-\nu_h)}{(1-2\nu_h)}, \text{ and} \tag{4}$$

$$\alpha = \sqrt{\frac{2\,S\phi}{3\,n(1-\phi)}}, \tag{5}$$

where

    ν_{grain} = Poisson's ratio of the grain, and
    ν_h = Poisson's ratio of gas hydrate,

$$\nu_{grain} = \frac{(3K_{grain} - 2\mu_{grain})}{2(3K_{grain} + \mu_{grain})}, \text{ and} \qquad (6a)$$

$$\nu_h = \frac{(3K_h - 2\mu_h)}{2(3K_h + \mu_h)}, \qquad (6b)$$

where

    K_{grain} = bulk modulus of the grain,
    μ_{grain} = shear modulus of the grain,
    K_h = bulk modulus of the gas hydrate, and
    μ_h = shear modulus of the gas hydrate.

Assuming that the Hydrate Ridge sediments are a mixture of sand and shale, if γ is the volumetric shale fraction, the grain moduli can be estimated by a Voigt-Reuss-Hill average of the moduli of sand and clay:

$$K_{grain} = \frac{1}{2}\left[\gamma K_{clay} + (1 - \gamma)K_{sand} + \frac{K_{sand}K_{clay}}{\gamma K_{sand} + (1 - \gamma)K_{clay}}\right], \qquad (7a)$$

and

$$\mu_{grain} = \frac{1}{2}\left[\gamma\mu_{clay} + (1 - \gamma)\mu_{sand} + \frac{\mu_{sand}\mu_{clay}}{\gamma\mu_{sand} + (1 - \gamma)\mu_{clay}}\right]. \qquad (7b)$$

Knowing from core analysis the actual range of sand and shale fractions for each site, we use a normalized gamma ray log to calculate γ.

According to Gassmann (1951), the in situ dry modulus of the sediments can be calculated from the measured in situ bulk modulus K by

$$K_{dry} = K_{grain}\frac{K[\phi(K_{grain} - K_{fluid}) + K_{fluid}] - K_{grain}K_{fluid}}{\phi K_{grain}(K_{grain} - K_{fluid}) + K_{fluid}(K - K_{grain})}, \qquad (8)$$

where

    K_{grain} = sediment grain bulk modulus and
    K_{fluid} = pore fluid bulk modulus.

K can be derived from the velocity and the density logs:

$$K = \rho\left(V_P^2 - \frac{4}{3}V_S^2\right). \qquad (9)$$

Using the velocity, density, and porosity logs and assuming that the pore fluid is only seawater, we use Equation 9 to calculate the in situ bulk modulus from the logs and Equation 8 to derive the dry bulk modulus of the Hydrate Ridge sediments. Starting from purely water-saturated sediments, we then increase hydrate saturation (S) in the expression of S_N (Equations 2–5) until the theoretical dry bulk modulus calculated with Equation 1 matches the measured dry bulk modulus. The values of the different parameters are given in Table T1.

T1. Parameter used in the elastic models, p. 38.

Free Gas Saturations

Below the BSR, the possible presence of free gas is indicated qualitatively by significantly lower V_P values. The saturation of free gas in the pore space can be calculated by fluid substitution in the Biot/Gassmann model (Gassmann, 1951; Murphy, 1984). In this model, the expression for the bulk modulus, from which Equation 8 is derived, is

$$K = K_{grain}\frac{K_{dry} + Q}{K_{grain} + Q}, \text{ with} \tag{10a}$$

$$Q = \frac{K_{fluid}(K_{grain} - K_{dry})}{\phi(K_{grain} - K_{fluid})}. \tag{10b}$$

Without knowledge of the fluid bulk modulus, which depends strongly on the unknown free gas saturation, one has to use a theoretical formulation to determine the dry frame modulus. Dvorkin et al. (1999) studied the effect of consolidation on the elastic properties of dry marine sediments and defined two regimes depending whether porosity is above a critical value (ϕ_c, usually 36%–40%). If porosity is above ϕ_c, which is the case in all sites drilled on Hydrate Ridge where porosities are consistently above 40%, the dry modulus is

$$K_{dry} = \left[\frac{3(1-\phi)/(1-\phi_c)}{3K_c + 4\mu_c} + \frac{3(\phi-\phi_c)/(1-\phi_c)}{4\mu_c}\right]^{-1} - \frac{4}{3}\mu_c, \tag{11}$$

where

K_c = dry bulk modulus at the critical porosity, and
μ_c = shear modulus at the critical porosity,

$$K_c = \left[\frac{Pn^2(1-\phi_c)^2\mu_{grain}^2}{18\pi^2(1-v_{grain})^2}\right]^{\frac{1}{3}}, \text{ and} \tag{12a}$$

$$\mu_c = 3K_c\frac{(5-4v_{grain})}{5(2-v_{grain})}, \tag{12b}$$

where

n = average number of grain contacts per grain (previously assumed to be 9), and
P = effective pressure.

If S_{gas} is the free gas saturation, the pore fluid bulk modulus can be estimated by a weighted average of the bulk moduli of the two phases present in the pore space (Murphy, 1984):

$$\frac{1}{K_{fluid}} = \frac{(1-S_{gas})}{K_{water}} + \frac{S_{gas}}{K_{gas}}. \tag{13}$$

A simple manipulation of Equation 10 provides an expression for K_{fluid} as a function of the saturated (K) and dry (K_{dry}) bulk moduli, which are derived, respectively, from the velocity and density logs (Equation 9) and from the porosity log (Equation 11). S_{gas} is then calculated from K_{fluid} by Equation 13.

Sonic Logging Waveform Amplitude

Guerin and Goldberg (2002) show that sonic logging waveforms display lower amplitudes in gas hydrate–bearing intervals. Empirical relationships and modeling of elastic wave propagation in hydrate-bearing sediments (Guerin and Goldberg, 2002; Guerin et al., 2005) suggest that the correlation between sonic attenuation and hydrate saturation is not strong enough to estimate qualitatively the low hydrate saturations (approximately <20%) typical of the intervals logged during Leg 204. However, the display of the waveform amplitudes alongside other logs

provides a qualitative indicator of gas hydrate occurrence. Low amplitudes are also traditionally associated with the presence of free gas (Murphy, 1982) and can be observed in several intervals below the BSR on Hydrate Ridge.

DATA AND RESULTS

For all the holes logged, we generated two different composite figures. The first is a summary of the STC analysis results of the different modes recorded during each sonic log pass. It provides a quality control assessment of the velocity data and also helps identify some of the loss of coherence that can be associated with free gas–bearing intervals. The second composite for each site combines the different logs associated with the sonic data and the presence of gas hydrate. The V_P and V_S logs and the sonic waveforms constitute our primary data. When available, we added the interval velocities calculated from the VSP and the comparison of the TvD relationships between the VSP and the synthetic seismograms. High resistivity values in the resistivity log are a qualitative indicator for the presence of gas hydrate, and the deep induction resistivity log is used to derive gas hydrate saturation estimates. The caliper log provides an assessment of the quality of the hole and of the reliability of the logs. The density log is combined with the V_P log to generate the synthetic seismogram and consequently can help identify some of the reflectors.

We highlight the panels with the main new results: the synthetic seismograms generated from the density and V_P logs are displayed as a function of depth to allow direct correlations between the logs and the seismic data; the gas hydrate and the free gas saturations derived from the cementation and the Gassmann models are compared with the estimates provided by the resistivity logs. These estimates are based on Archie's law and are calculated with the method described by Collett (1998), applied to the deep induction wireline resistivity log for each hole. The resulting water saturations can be interpreted in terms of gas hydrate or free gas saturation depending on the location within or outside the gas hydrate stability zone.

In order to illustrate these correlations and their implications for the Hydrate Ridge system, we superimpose each synthetic seismogram on a short east-west section of the 3-D seismic survey. The results are discussed from the west flank sites (Holes 1245E and 1247B) through the crest (Hole 1250F) to the eastern flank (Hole 1244E) and the eastern basin (Holes 1252A and 1251H) (see Fig. F1 for locations).

Hole 1245E

Figure F6 shows that, despite the irregular hole conditions (see caliper in Fig. F7), the monopole and lower dipole waveforms displayed strong coherence overall, allowing us to draw reliable velocity logs. However, as a result of the irregular hole and of the low variability in the data, both the sonic and density logs are noisy and combine to produce only an adequate synthetic seismogram. The comparison of the seismogram with the seismic data and the logs in Figure F7 still allows us to identify the main reflectors in Hole 1245E: the BSR at 130 meters below seafloor (mbsf) and Horizon A at 180 mbsf. However, the amplitude of these reflections in the synthetic seismogram is significantly lower than in the seismic data. Both reflections in the synthetic seismo-

F6. Slowness-time coherence analysis of sonic logging waveforms in Hole 1245E, p. 23.
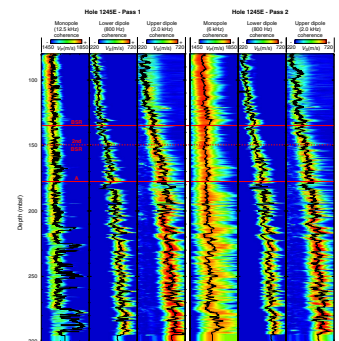
F7. Wireline logs associated with the presence of gas hydrate in Hole 1245E, p. 24.
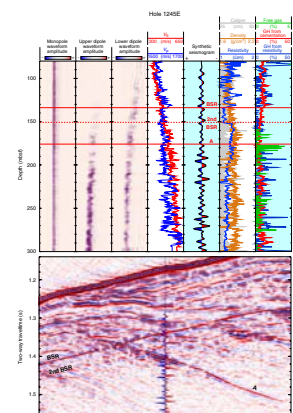
gram are generated by slight decreases in V_P, attributed to the bottom of the gas hydrate stability zone for the BSR and to the presence of free gas within the volcanic glass–rich sediments and ashes that constitute Horizon A (Tréhu, Bohrmann, Rack, Torres, et al., 2003). The low amplitude of the synthetic reflections might also indicate that some of the free gas responsible for the reflections in the 3-D seismic data escaped during drilling and prior to the recording of the sonic logs. As one of the main conduits for gas into the Hydrate Ridge gas hydrate system, and despite possible escape of free gas, Horizon A is still the location of the highest free gas saturation identified by the Gassmann model. Another strong reflection at ~150 mbsf coincides with the "double BSR" at 1.37 s two-way traveltime (TWT) described by Bangs et al. (2005). In Hole 1245E, this reflection corresponds to a steplike increase in the resistivity log. Although there is no indication of a lithologic change associated with this resistivity increase, it seems to mark the top of the occurrence of free gas indicated by the Gassmann model. The lower monopole waveform amplitudes and the results of the Gassmann model suggest that free gas is pervasively present below this depth.
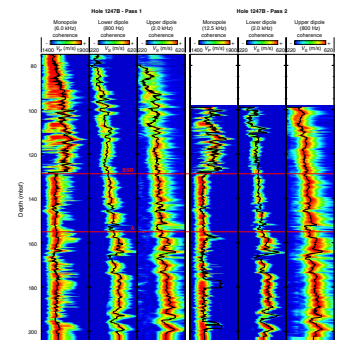
Gas hydrate saturations predicted by the cementation theory above the BSR are overall similar to the values predicted from the resistivity log by Archie's law but suggest a more uniform distribution (Fig. F7). Below the bottom of the gas hydrate stability zone, the presence of gas hydrate suggested by the cementation model is likely an artifact resulting from the lithological variability and the deformed nature of the sediments, which are not taken into account in the model.

Hole 1247B

The high coherence of the sonic waveforms (Fig. F8) and the smooth caliper log in Figure F9 show that Hole 1247B was in excellent condition despite the poorly consolidated nature of the Hydrate Ridge sediments. As a result, all logs are of very good quality and the synthetic seismogram clearly identifies the BSR at 128 mbsf, Horizon A at 153 mbsf, and most of the other reflectors. The amplitude of Horizon A is again lower in the synthetic trace than in the seismic data, which could also be attributed to the escape of some of the original free gas present in this interval. The favorable hole conditions also allowed a strong coupling of the geophones at most attempted stations of the VSP. The good agreement between the traveltimes derived from the synthetic seismogram and from the VSP validates these two independent data sets. However, despite the good hole conditions and data quality, the interval velocity values derived from the VSP are noticeably higher than the V_P log below the BSR. Considering the overall narrow range of the V_P values, this does not affect the good agreement between the TvD relationships. This discrepancy could suggest some local effect due to the heterogeneous distribution of free gas and the differences between the tools. While the DSI waveforms travel in close vicinity to the borehole, the VSP shots travel from the surface to the downhole geophone and are less sensitive to local free gas occurrences over their path. In Figure F8, the wide coherence peaks in the monopole waveforms below Horizon A also suggest some arrivals faster than the ones picked with the highest coherence, indicating the possible influence of an heterogeneous free gas distribution.

The sharp drop in V_P that generates the BSR, typical of the traditional representation of gas hydrate reservoirs, is mostly due to the high gas

F8. Slowness-time coherence analysis of sonic logging waveforms in Hole 1247B, p. 25.

F9. Wireline logs associated with the presence of gas hydrate in Hole 1247B, p. 26.
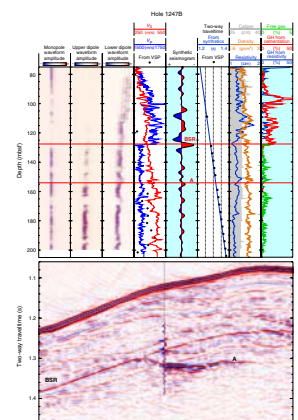
hydrate saturation indicated by the results of the cementation theory. The presence of gas hydrate is surprisingly less apparent in the resistivity log, and although both hydrate saturation curves provide similar values near 20% of the pore space, the hydrate saturation derived from the sonic log is overall higher and more uniform than predicted by Archie's method. Only a few gas hydrate samples were recovered from the core at this site (Tréhu, Bohrmann, Rack, Torres, et al., 2003), but the presence of strong chlorinity anomalies (Tréhu et al., 2004b) supports the sonic log indication of significant amounts of gas hydrate immediately above the BSR. This is also consistent with the location of Hole 1247B near the crest of southern Hydrate Ridge, where the highest hydrate saturations have been observed, and with the presence of a very clear BSR (Fig. F9).

In agreement with the observations of Guerin and Goldberg (2002), all waveform amplitudes are significantly lower above the BSR, and the effect of gas hydrate on waveform amplitude is stronger on the upper dipole waveforms than on the lower dipole because of the higher source frequency of the upper dipole source.

Below the BSR, the Gassmann model indicates consistent amounts of free gas, with the highest saturations (~1.5%) between 165 and 170 mbsf, 10 m below Horizon A. This coincides with significantly lower amplitudes in the logging waveforms. Similar correlation between significant free gas occurrence and low amplitudes is observed in several intervals below the BSR.
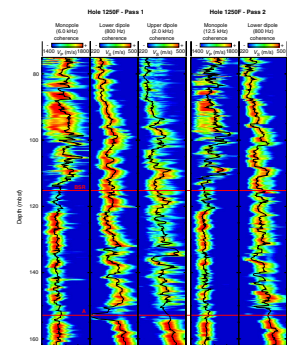
Hole 1250F

As in Hole 1247B, the high waveform coherence in Figure F10 and the caliper log in Figure F11 indicate very good hole conditions and very reliable logging data in Hole 1250F. Accordingly, the synthetic seismogram reproduces all the most significant reflectors, including the BSR at ~115 mbsf and Horizon A at 152 mbsf. The resulting TvD relationship is also in good agreement with the transit times measured by the VSP.

Gas hydrate saturations calculated from the sonic log by the cementation theory indicate values similar to the results of Archie's law but suggest a less uniform distribution and significant saturations all the way to the BSR, whereas the resistivity log does not identify any gas hydrate below ~105 mbsf. The absence of strong chlorinity or infrared anomalies immediately above the BSR (Tréhu, Bohrmann, Rack, Torres, et al., 2003; Tréhu et al., 2004b) also supports the absence of gas hydrate in this interval. This contradiction between the resistivity and the V_P log can be due partially to the different tool geometries, orientations, and energy paths. It is also an indication of the highly heterogeneous gas hydrate distribution at the crest of Hydrate Ridge. The V_P log and the saturation model results show clearly, as in Hole 1247B, that the BSR marks the shallowest occurrence of free gas. Milkov et al. (2004) and Tréhu et al. (2004a) suggest that, because of the excess input of free gas in the system, free gas and gas hydrate might coexist above the BSR. The consistently high V_P values above the BSR seem to contradict this interpretation or to indicate a more complex interplay between the heterogeneous gas hydrate and free gas distributions in this active system.

Despite the consistent presence of free gas identified by the Gassmann model below the BSR, this model fails to identify free gas in Horizon A in Hole 1250F. By comparison, Tréhu et al. (2004a) use the

F10. Slowness-time coherence analysis of sonic logging waveforms in Hole 1250F, p. 28.

F11. Wireline logs associated with the presence of gas hydrate in Hole 1250F, p. 29.

G. Guerin et al.
Sonic Velocities in an Active Gas Hydrate System

11
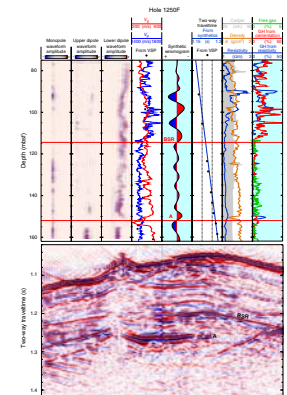
logging-while-drilling (LWD) density logs to estimate very high (>50%) free gas saturations in this horizon, which is supported by a crossover of low density and low neutron porosity in the LWD logs (Tréhu, Bohrmann, Rack, Torres, et al., 2003). The low dipole waveforms amplitude and coherence in this interval also support the presence of free gas and the interpretation of Horizon A as the main free gas conduit to the system (Tréhu, Bohrmann, Rack, Torres, et al., 2003; Tréhu et al., 2004a). The absence of a decrease in V_P indicates that most of the free gas present might have escaped by the time of the sonic log, which does not affect the LWD measurements made immediately after the bit penetration. The strong decrease in V_S in Horizon A suggests that there might have been an elevated pressure in Horizon A before drilling and that, considering the poorly consolidated nature of the sediments, the pore fluid was carrying most of the burden. As the gas and the pressure were released by drilling, the matrix collapsed and lost part of its cohesion and shear strength, generating a decrease in V_S.
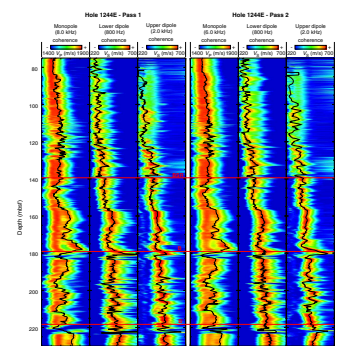
Hole 1244E

The strong waveform coherence for all the passes and modes in Figure F12 and the almost perfect caliper log in Figure F13 indicate that all the wireline logs recorded in Hole 1244E were of excellent quality. Figure F13 also shows that Hole 1244E was the only location on Hydrate Ridge where it was possible to obtain good coupling for the VSP at every attempted depth, every 5 m. Accordingly, the interval velocities derived from the VSP and the V_P log are in excellent agreement, as well as the TvD relationships derived from the VSP and the synthetic seismogram. In addition to the very clear direct arrivals, the VSP waveforms in Figure F4 also feature the reflection of the most prominent reflector at this site: Horizon B' at ~217 mbsf. The other reflectors identified by correlation between the synthetic seismogram and the seismic data are Horizon B at ~180 mbsf and the BSR at ~140 mbsf. The good agreement between the TvD relationships suggests that the BSR is deeper by 11 m than estimated by Tréhu, Bohrmann, Rack, Torres, et al. (2003).

Archie's relationship and the cementation theory applied to the resistivity and sonic logs indicate lower hydrate saturations in Site 1244 than in the crest sites. This observation is supported by the fact that Site 1244 is located to the east of Hydrate Ridge (Fig. F1), away from the main gas hydrate accumulation fed by Horizon A. All estimates suggest a fairly uniform gas hydrate saturation around 15% of the pore space above the BSR. A reflection at 90 mbsf, or 1.32 s TWT, coincides with the bottom of an interval with higher resistivity, where the Archie relationship predicts gas hydrate saturation values significantly higher than the results of the cementation model. Correlation between the synthetic seismogram and the seismic line shows that this interval also displays higher seismic reflectivity, which is an apparent contradiction with high gas hydrate saturations (Guerin and Goldberg, 2002). The slightly higher density in this interval, also contradictory with high hydrate saturations, indicates that the resistivity increase is not due uniquely to the presence of gas hydrate but possibly to some different lithology, although this was not identified in the core observation (Tréhu, Bohrmann, Rack, Torres, et al. 2003).

The lower V_P values and the loss of waveform coherence in several short intervals between Horizons B and B' suggest the presence of free gas, which is identified by the Gassmann model and also indicated by

F12. Slowness-time coherence analysis of sonic logging waveforms in Hole 1244E, p. 30.

F13. Wireline logs associated with the presence of gas hydrate in Hole 1244E, p. 31.
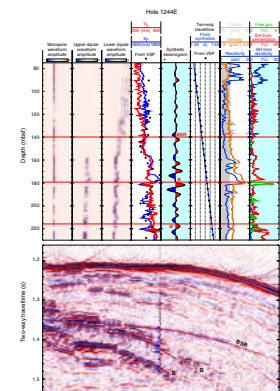
the low monopole waveform amplitudes in discrete intervals. The highest gas saturations are measured within Horizon B, indicating that this turbiditic horizon also contributes to the gas hydrate accumulation at the crest of Hydrate Ridge, as well as the volcanic glass-rich Horizon B′.

As in Hole 1245E, the suggestion by the cementation model of gas hydrate below the bottom of the gas hydrate stability zone is an artifact resulting from the overall low gas hydrate saturations and the lithological variability and deformed nature of the sediments. In particular, between 160 and 180 mbsf, the increase in velocity responsible for the apparent gas hydrate occurrence is due to a decrease in porosity, indicated by the higher resistivity and density, which likely reflects a local deformation immediately above Horizon B.
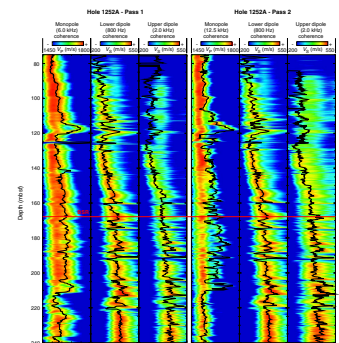
Hole 1252A

Figure F14 shows that the higher frequency upper dipole waveform displays only a weak coherence in the upper section of Hole 1252A, as well as the high frequency monopole waveforms in the deeper section (Pass 2). However, all the V_P and V_S logs agree well between the different passes and sources, suggesting that the sonic logs are of good quality, despite the low amplitudes shown in Figure F15. Drilled on the western flank of a secondary anticline east of Hydrate Ridge, Hole 1252A is located where the BSR within the accretionary core of the anticline intersects the overlying sediments of Hydrate Ridge's eastern flank (see the seismic section in Fig. F15). As a result of this deformation, the sediments are likely to be less cohesive, which is confirmed by the very irregular caliper in Figure F15. However, the hole enlargements never exceed the maximum reach of the tools. As another consequence of the local deformation, the BSR is interrupted on the seismic line near the well location and can only be correlated to a weak reflector in the synthetic seismogram at ~165 mbsf. The strongest reflector in the seismogram is generated by the high velocity and density in a series of glauconitic sand layers between 115 and 120 mbsf, at the contact between the anticline core and the overlaying sediments.

Below the BSR, the V_P log shows a slightly decreasing trend with depth, opposite to a normal consolidation profile within these disturbed sediments. Because this trend does not occur in the deformed sediments above the BSR, this suggests that the presence of gas hydrate might contribute to the consolidation of the sediments above the BSR.

Gas hydrate saturations derived from the elastic logs indicate a relatively uniform gas hydrate distribution, increasing slightly downhole to a maximum value of ~10% of the pore space at the BSR. The resistivity log suggests a more heterogeneous gas hydrate distribution, indicating in particular some high-saturation intervals between 80 and 100 mbsf, in the undeformed sediments above the glauconitic sands. Only few indications of gas hydrate were observed in the recovered cores, but several infrared camera anomalies suggested that any gas hydrate present had to be disseminated (Tréhu, Bohrmann, Rack, Torres, et al., 2003). The low dipole waveform amplitudes above the BSR tend to support the prediction of the cementation model of a significant disseminated gas hydrate distribution (Guerin and Goldberg, 2002). The high saturations derived by the cementation theory within the glauconite-rich sands and the apparent hydrate presence below the BSR by the resistivity and the elastic logs are indications that these highly disturbed sediments present a consolidation state distinctly different from the normal pore space configuration assumed in the cementation theory and possibly in

F14. Slowness-time coherence analysis of sonic logging waveforms in Hole 1252A, p. 33.

F15. Wireline logs associated with the presence of gas hydrate in Hole 1252A, p. 34.
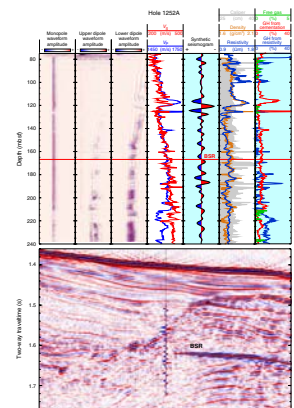
Archie's law. Similarly, the apparent presence of gas hydrate suggested by the cementation model below the bottom of the gas hydrate stability zone is also a consequence of the deformed nature of the sediments. By comparison, the Gassmann model, which makes no assumption on the pore scale grain interactions, predicts some possibly significant gas presence in a low-velocity interval between 210 and 220 mbsf. The low sonic waveform amplitudes in this interval support the presence of free gas, which was not identified previously.

Hole 1251H

The results of the STC analysis of all the waveforms recorded in Hole 1251H in Figure F16 indicate consistently low velocity and low dipole waveform coherence over the entire interval logged, characteristic of poorly consolidated sediments. In particular, V_S values are so low that the 20-ms window used to record the dipole waveforms was too short to capture the flexural waves above ~105 mbsf. The irregular caliper log in Figure F17 indicates that the bad hole conditions could be responsible for some loss in waveform amplitude and coherence. In particular, the high-frequency upper dipole waveform in Figure F17 seems to have been particularly affected by the hole conditions. But the low quality of the borehole, and consequently of some of the waveforms, mostly underlines the poorly consolidated nature of the sediments. Although the hole was drilled to 445 mbsf, the unstable formation caused obstructions to form and the hole to collapse in the deeper section, so that no sonic data were recorded below 185 mbsf, ~10 m above the BSR (Tréhu, Bohrmann, Rack, Torres, et al., 2003). The enlarged hole and the lack of cohesion of the sediments also prevented a good mechanical coupling between the formation and the VSP tool so that waveforms were recorded successfully only at four stations (Fig. F5). As another consequence of the enlarged hole, the density log was of bad quality in intervals where the hole was too large for the tool to make contact with the formation. Consequently, we used the density measured on core samples to generate the synthetic seismogram (Fig. F17).

Despite the difficult hole conditions, the other logging data recorded in Hole 1251H were of good quality and the synthetic seismogram reproduces well most of the reflectors penetrated by the well. The TvD relationship derived from the sonic log and the seismic/synthetics correlation is also in good agreement with the check shots provided by the VSP. In the absence of a BSR, the most significant reflector for the log/seismic correlation is generated by the angular unconformity at 1.78 s TWT, which was identified in the cores at ~130 mbsf. The brightest reflector in the seismic line and in the synthetic seismogram corresponds to a bed dipping to the east at 1.81 s TWT that is generated in the synthetic seismogram by an interval with reduced V_P between 143 and 148 mbsf. This interval does not correspond to any lithology change in the cores (Tréhu, Bohrmann, Rack, Torres, et al., 2003) but is also characterized by low dipole waveform amplitudes. The low V_P and dipole amplitude, as well as the brightness of the reflector, suggest a possible presence of free gas within the gas hydrate stability field, similar to observations by Guerin et al. (1999). However, the simultaneous presence of gas hydrate and free gas changes the sediment frame properties, so the Gassmann model does not detect any free gas.

The cementation theory predicts a steady increase in gas hydrate saturation with depth, from 0% to ~10% of the pore space, whereas the re-

F16. Slowness-time coherence analysis of sonic logging waveforms in Hole 1251H, p. 35.
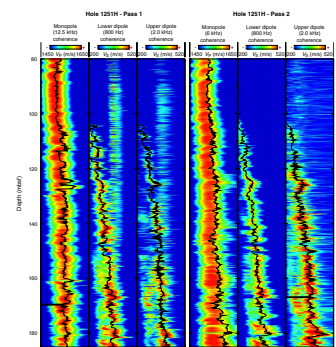
F17. Wireline logs associated with the presence of gas hydrate in Hole 1251H, p. 36.
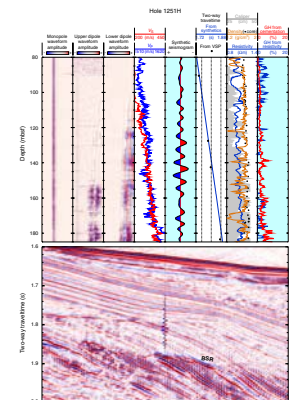
sistivity log suggests somewhat higher values in a few discrete intervals. The discrepancy between the two methods could be partially due to the hole conditions and to the difference between the geometry of investigation of the two tools in an overall heterogeneous hydrate distribution. However, the high gas hydrate saturation at the bottom of the interval indicated by the cementation theory agrees with the strong infrared and chlorinity anomalies observed immediately above the BSR in adjacent Holes 1251A and 1251D (Tréhu, Bohrmann, Rack, Torres, et al., 2003; Tréhu et al., 2004b).

SUMMARY

We have combined all the in situ sonic measurements made on Hydrate Ridge during Leg 204 in order to draw a complete overview of the implications of these data for the Hydrate Ridge system. The synthetic seismograms, calibrated or not by the VSP, enable a clear correlation between specific features in the logs and distinct reflections in the 3-D seismic data set. In addition to the BSR, the most significant reflectors are the various horizons below the gas hydrate stability field that contribute to the gas supply of the gas hydrate reservoir. Horizon A is the main free gas conduit, but Horizons B and B′ also display significant amounts of free gas. The Gassmann model also suggests a pervasive presence of free gas under the southern Hydrate Ridge summit.

The sonic logs also provide new estimates of gas hydrate saturations that agree overall with predictions based on the resistivity logs but differ in the details of the distribution. The different methods indicate an overall gas hydrate saturation of 10%–20% near the crest of southern Hydrate Ridge, decreasing to ~5% on the flanks. When present below the BSR, free gas saturation does not exceed a few percent of the pore space.

The cementation model used in this study is by no means the only formulation to derive gas hydrate saturations from velocity logs, and other models could possibly provide more reliable estimates. In particular, the suggestion of gas hydrate below the bottom of the gas hydrate stability field in several holes is obviously inaccurate because it is thermodynamically impossible and is a clear indication of the limits of this formulation. Guerin et al. (1999) successfully used this model in a significantly different environment, Blake Ridge, which is a passive margin where the penetrated sediments had an almost uniform lithology. Such description does not apply to the Hydrate Ridge sediments, which have a more diverse composition and, more significantly, are being actively deformed. The reasons why we chose this model for this study was its ease of use, its apparent accuracy in the previous study, and the fact that, unlike other effective media models, it offers a physical description of the grain-scale interaction between grains and hydrate. Its failure at more reliably identifying gas hydrate on Hydrate Ridge shows that the assumption that the gas hydrate/cement forms uniformly on spherical grains is an oversimplification of hydrate distribution and of the pore space. Guerin and Goldberg (2005) show that cementation occurs in the presence of gas hydrate but that friction between gas hydrate and the grains is responsible for the energy dissipation measured. Such friction implies that pore scale distribution is heterogeneous, which is hardly compatible with a uniform coating of grains by gas hydrate.

However, our goals were to provide not only a general overview of the implications of the acoustic logs on Hydrate Ridge, including new

independent gas hydrate estimations to complement existing estimates, but also the integration of the logs and of the VSP with the seismic data, rather than a study of different possible models to determine gas hydrate saturations from acoustic logs. The overall agreement between the estimates derived from the resistivity and the velocity logs within the gas hydrate stability zone shows that it provides a reasonable estimate of global gas hydrate saturation, which has been shown to vary significantly between authors (Milkov et al., 2003).

Finally, the sonic logging waveforms offer a qualitative indication of the presence of gas hydrate and free gas. The sonic amplitudes are strongly dependent on the nature and the frequency of the source, and the high frequency dipole appears to be the most sensitive in this low-hydrate saturation environment.

The agreement between the different indicators described is best in the crest sites, in Holes 1247B and 1250F, which are the sites with the highest gas hydrate saturations. This suggests that the effect of gas hydrate on sonic velocity through cementation, and more significantly on sonic attenuation, requires significant amounts of gas hydrate. Surprisingly, although Site 1247 is located near the top of the mound, and the BSR is clearly present at this site, very little gas hydrate was recovered in the cores during Leg 204. The hydrate saturations derived from the elastic logs indicate significant values that were not identified at the time of drilling. Similarly, at Site 1250, the resistivity logs indicate low hydrate saturations immediately above the BSR whereas the bulk modulus and the elastic properties suggest high saturations, which are necessary to generate such a strong BSR. These two sites have the most clearly defined BSR of the visited sites. Overall, the results confirm that accurate identification of gas hydrate can be made only by the combination of various measurements in order to properly estimate the effect of heterogeneous free gas and gas hydrate distribution on the elastic and electrical properties of the formation.

ACKNOWLEDGMENTS

REFERENCES

Bangs, N.L.B., Musgrave, R.J., and Tréhu, A.M., 2005. Upward shifts in the southern Hydrate Ridge gas hydrate stability zone following postglacial warming, offshore Oregon. *J. Geophys. Res.,* 110. **doi:10.1029/2004JB003293**

Collett, T.S., 1998. Well log evaluation of gas hydrate saturations. In *Trans. SPWLA 39th Annu. Logging Symp.:* Houston (SPWLA), 39:MM.

Dvorkin, J., and Nur, A., 1996. Elasticity of high-porosity sandstones: theory for two North Sea data sets. *Geophysics,* 61:1363–1370. **doi:10.1190/1.1444059**

Dvorkin, J., Nur, A., and Yin, H., 1994. Effective properties of cemented granular materials. *Mech. Mater.,* 18(4):351-366. **doi:10.1016/0167-6636(94)90044-2**

Dvorkin, J., Prasad, M., Sakai, A., and Lavoie, D., 1999. Elasticity of marine sediments: rock physics modeling. *Geophys. Res. Lett.,* 26:1781–1784. **doi:10.1029/1999GL900332**

Gassmann, F., 1951. Elastic waves through a packing of spheres. *Geophysics,* 15:673–685. **doi:10.1190/1.1437718**

Guerin, G., and Goldberg, D., 2002. Sonic waveform attenuation in gas hydrate–bearing sediments from the Mallik 2L-38 research well, MacKenzie Delta, Canada. *J. Geophys. Res.,* 107:2088. **doi:10.1029/2001JB000556**

Guerin, G., and Goldberg, D., 2005. Modeling of acoustic wave dissipation in gas hydrate–bearing sediments. *Geochem., Geophys., Geosyst.,* 6. **doi:10.1029/2005GC000918**

Guerin, G., Goldberg, D., and Collett, T.S., 2005. Sonic attenuation in the Mallik 5L38 gas hydrate research well. *Bull.—Geol. Surv. Can.,* 585.

Guerin, G., Goldberg, D., and Meltser, A., 1999. Characterization of in situ elastic properties of gas-hydrate bearing sediments on the Blake Ridge. *J. Geophys. Res.,* 104:17781–17796. **doi:10.1029/1999JB900127**

Harrison, A.R., Randall, C.J., Aron, J.B., Morris, C.F., Wignall, A.H., Dworak, R.A., Rutledge, L.L., and Perkins, J.L., 1990. Acquisition and analysis of sonic waveforms from a borehole monopole and dipole source for the determination of compressional and shear speeds and their relation to rock mechanical properties and surface seismic data. *Abstract 65, Ann. Tech. Conf. Exhib. Soc. Pet. Eng.,* 23–26/9, 267–282.

Helgerud, M.B., Dvorkin, J., Nur, A., Sakai, A., and Collett, T., 1999. Elastic-wave velocity in marine sediments with gas hydrates: effective medium modeling. *Geophys. Res. Lett.,* 26(13):2021–2024. **doi:10.1029/1999GL900421**

Kimball, C.V., and Marzetta, T.L., 1984. Semblance processing of borehole acoustic array data. *Geophysics,* 49:274–281. **doi:10.1190/1.1441659**

Lee, M.W., and Collett, T.S., 2005. Assessment of gas hydrate saturations estimated from sonic logs in the Mallik 5L-38 well, Canada. *In* Dallimore, S.R., and Collett, T.S. (Eds.), *Scientific Results from the Mallik 2002 Gas Hydrate Production Well Program, Mackenzie Delta, Northwest Territories, Canada.* Bull.—Geol. Surv. Can., 585.

Lee, M.W., Hutchinson, D.R., Collett, T.S., and Dillon, W.P., 1996. Seismic velocities for hydrate-bearing sediments using weighted equation. *J. Geophys. Res.,* 101:20347–20358. **doi:10.1029/96JB01886**

Milkov, A.V., Claypool, G.E., Lee, Y.-J., Xu, W., Dickens, G.R., Borowski, W.S., and the ODP Leg 204 Scientific Party, 2003. In situ methane concentrations at Hydrate Ridge offshore Oregon: new constraints on the global gas hydrate inventory from an active margin. *Geology,* 31:833–836.

Milkov, A.V., Dickens, G.R., Claypool, G.E., Lee, Y.-J., Borowski, W.S., Torres, M.E., Xu, W., Tomaru, H., Tréhu, A.M., and Schultheiss, P., 2004. Co-existence of gas hydrate, free gas, and brine within the regional gas hydrate stability zone at Hydrate Ridge (Oregon margin): evidence from prolonged degassing of a pressurized core. *Earth Planet. Sci. Lett.,* 222:829–843. **doi:10.1016/j.epsl.2004.03.028**

Murphy, W.F., 1982. Effects of partial water saturation on attenuation in Massilon sandstone and Vycor porous glass. *J. Acoust. Soc. Am.,* 71:1458–1468.

Murphy, W.F., 1984. Acoustic measures of partial gas saturation in tight sandstones. *J. Geophys. Res.,* 89:11549–11559.

Peterson, R.A., Fillipone, W.R., and Coker, E.B., 1955. The synthesis of seismograms from well log data. *Geophysics,* 20:516–538. **doi:10.1190/1.1438155**

Tréhu, A.M., and Bangs, N., 2001. 3-D seismic imaging of an active margin hydrate system, Oregon continental margin, report of cruise TTN112. *Oregon State Univ. Data Rpt.,* 182.

Tréhu, A.M, Bohrmann, G., Rack, F.R., Torres, M.E., et al., 2003. *Proc. ODP, Init. Repts.,* 204 [Online]. Available from World Wide Web: <**http://www-odp.tamu.edu/pub-lications/204_IR/204ir.htm**>. [Cited 2006-08-30]

Tréhu, A.M., Flemings, P.B., Bangs, N.L., Chevallier, J., Gràcia, E., Johnson, J.E., Liu, C.S., Riedel, M., and Torres, M.E., 2004a. Feeding methane vents and gas hydrate deposits at south Hydrate Ridge. *Geophys. Res. Lett.,* 31:L23310. **doi:10.1029/ 2004GL021286**

Tréhu, A.M., Long, P.E., Torres, M.E., Bohrmann, G., Rack, F.R., Collett, T.S., Goldberg, D.S., Milkov, A.V., Riedel, M., Schultheiss, P., Bangs, N.L., Barr, S.R., Borowski, W.S., Claypool, G.E., Delwiche, M.E., Dickens, G.R., Gracia, E., Guerin, G., Holland, M., Johnson, J.E., Lee, Y.-J., Liu, C.-S., Su, X., Teichert, B., Tomaru, H., Vanneste, M., Watanabe, M., and Weinberger, J.L., 2004b. Three-dimensional distribution of gas hydrate beneath southern Hydrate Ridge: constraints from ODP Leg 204. *Earth Planet. Sci. Lett.,* 222:845–862. **doi:10.1016/j.epsl.2004.03.035**

Wuenschel, P.C., 1960. Seismogram synthesis including multiples and transmission coefficients. *Geophysics,* 25:106–129. **doi:10.1190/1.1438677**

Figure F1. Map of southern Hydrate Ridge, offshore Oregon, and location of the sites where sonic logs were recorded during Leg 204. The red straight lines across each site indicate the extent of the 3-D seismic data displayed for each site in subsequent figures.
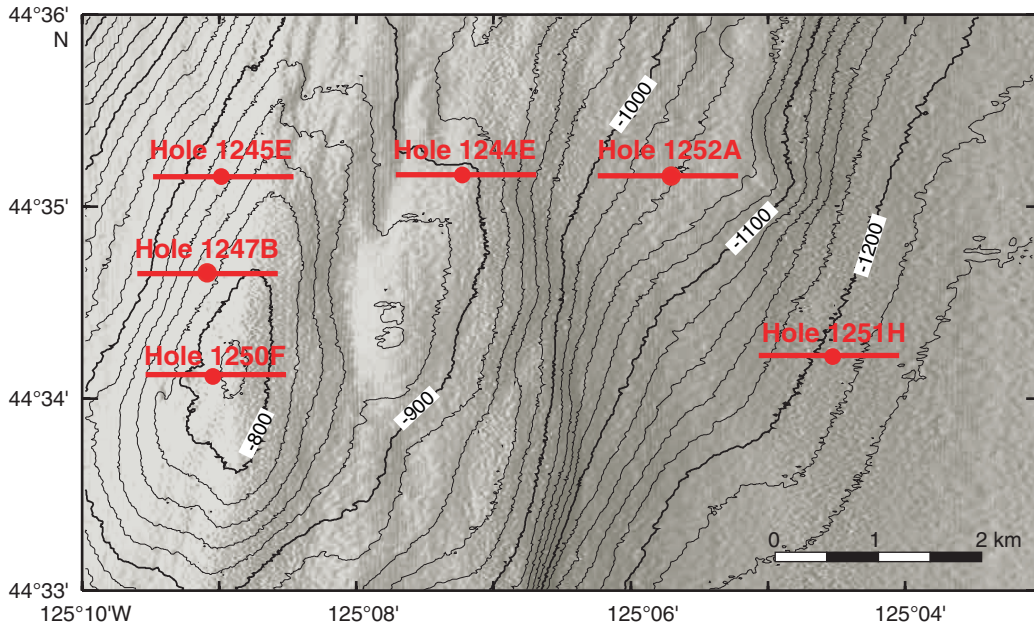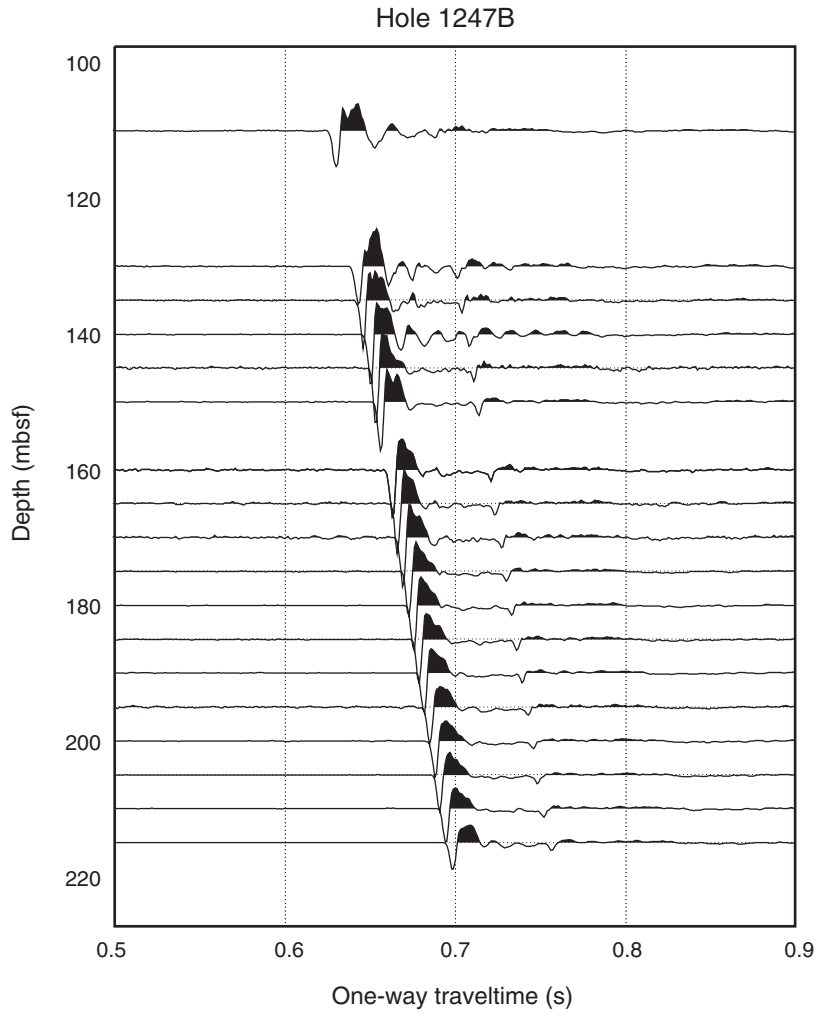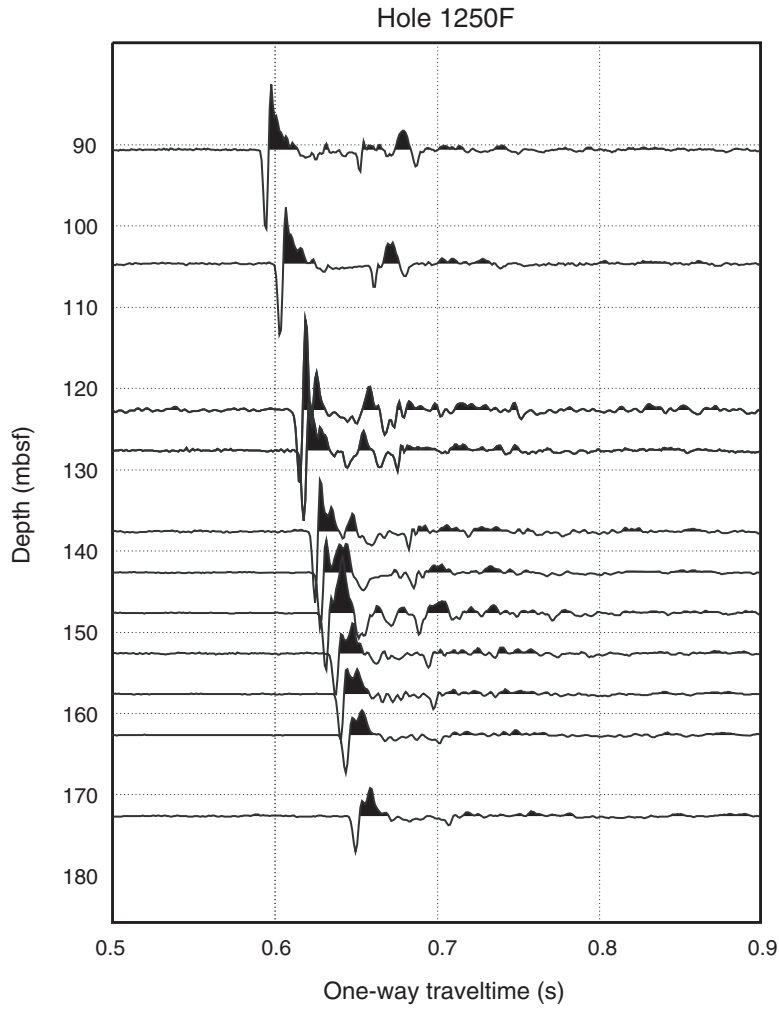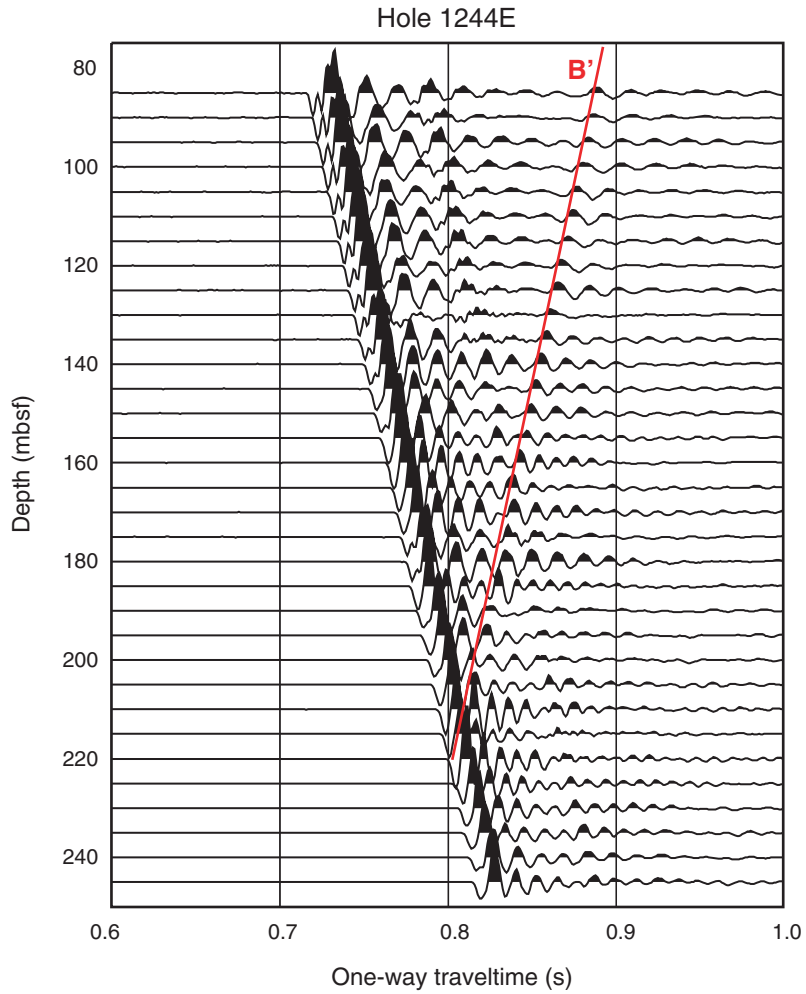
Figure F2. Stacked waveforms of the VSP recorded in Hole 1247B. The waveforms have not been corrected for the position of the source and the triggering delay, and the traveltime is not the actual transit time used in the TvD relationship. BSR = bottom-simulating reflector.

Figure F3. Stacked waveforms of the VSP recorded in Hole 1250F. The waveforms have not been corrected for the position of the source and the triggering delay, and the traveltime is not the actual transit time used in the TvD relationship.

Figure F4. Stacked waveforms of the VSP recorded in Hole 1244E. The waveforms have not been corrected for the position of the source and the triggering delay, and the traveltime is not the actual transit time used in the TvD relationship. B′ = Horizon B′.

Figure F5. Stacked waveforms of the VSP recorded in Hole 1251H. The waveforms have not been corrected for the position of the source and the triggering delay, and the traveltime is not the actual transit time used in the TvD relationship.

Hole 1251H
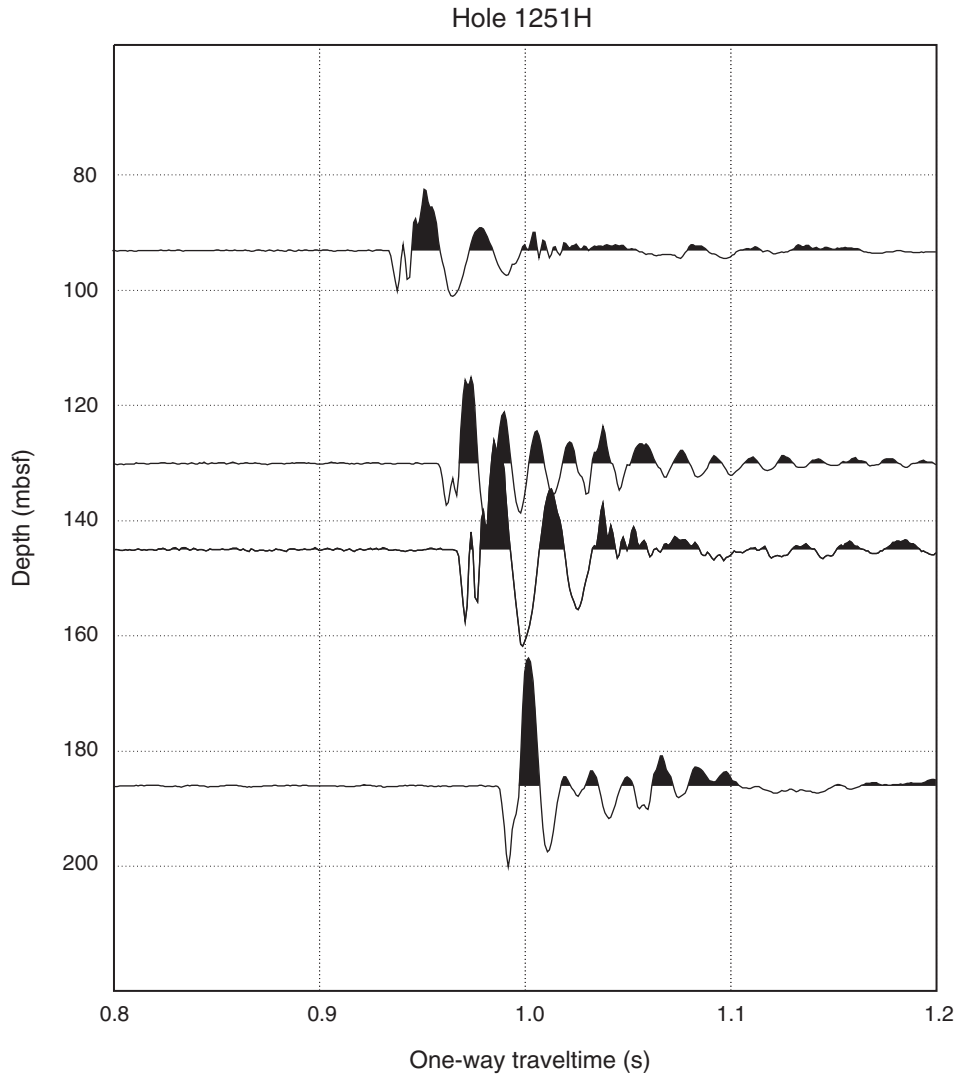
Figure F6. Results of the slowness-time coherence analysis of all the sonic logging waveforms recorded in Hole 1245E to derive the velocity logs. The colors indicate the coherence across the eight-receiver array corresponding to any velocity integrated over the entire time window. The black line indicates the final result. The gray dots indicate local maxima in coherence that could be interpreted as arrivals. BSR = bottom-simulating reflector, A = Horizon A.
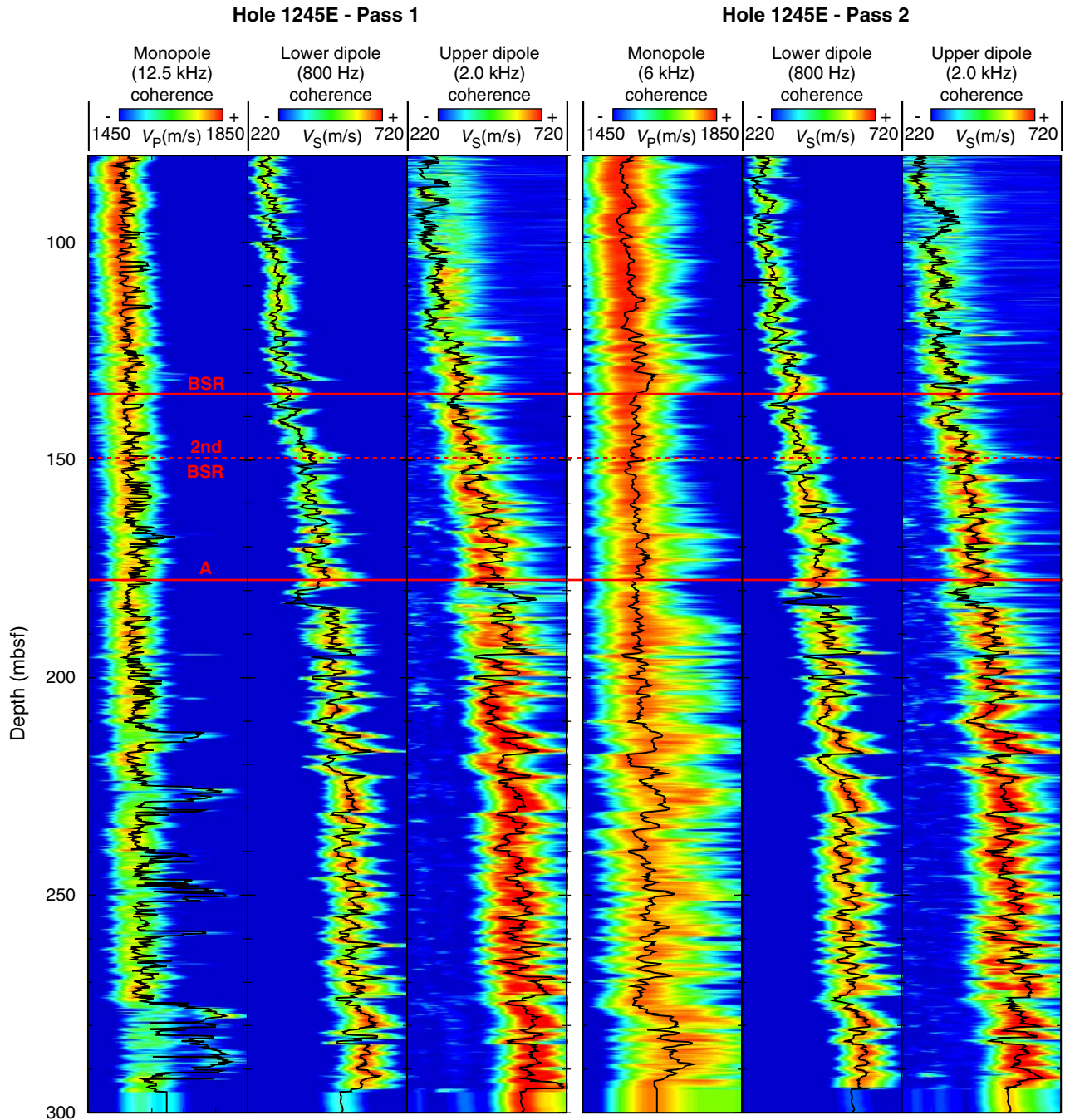
Figure F7. Wireline logs associated with the presence of gas hydrate (GH) in Hole 1245E. The synthetic seismogram and the gas hydrate concentration profiles were calculated from these logs. The synthetic seismogram is superimposed on a short east-west transect of the 3-D seismic survey for identification of the reflectors. BSR = bottom-simulating reflector, A = Horizon A.
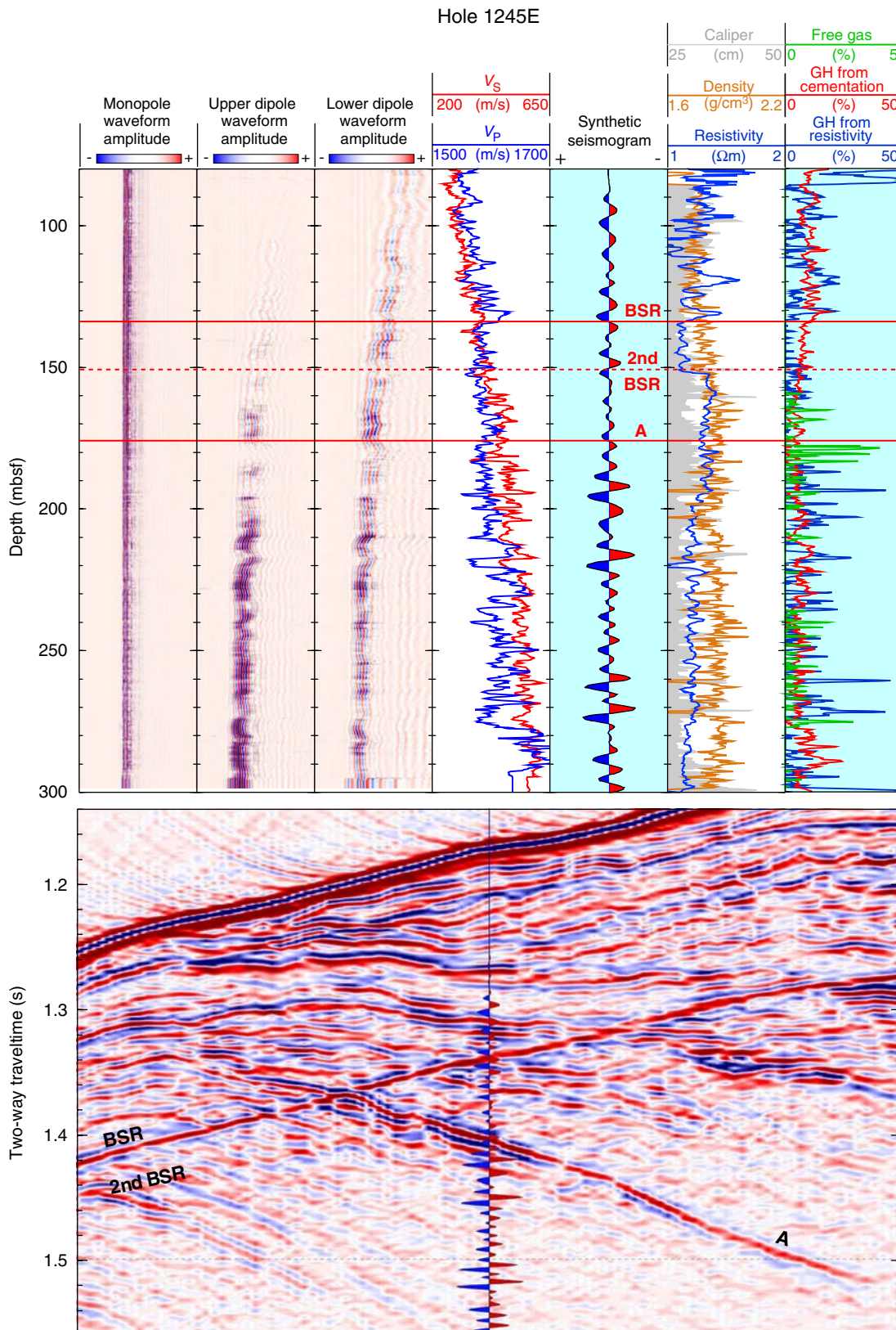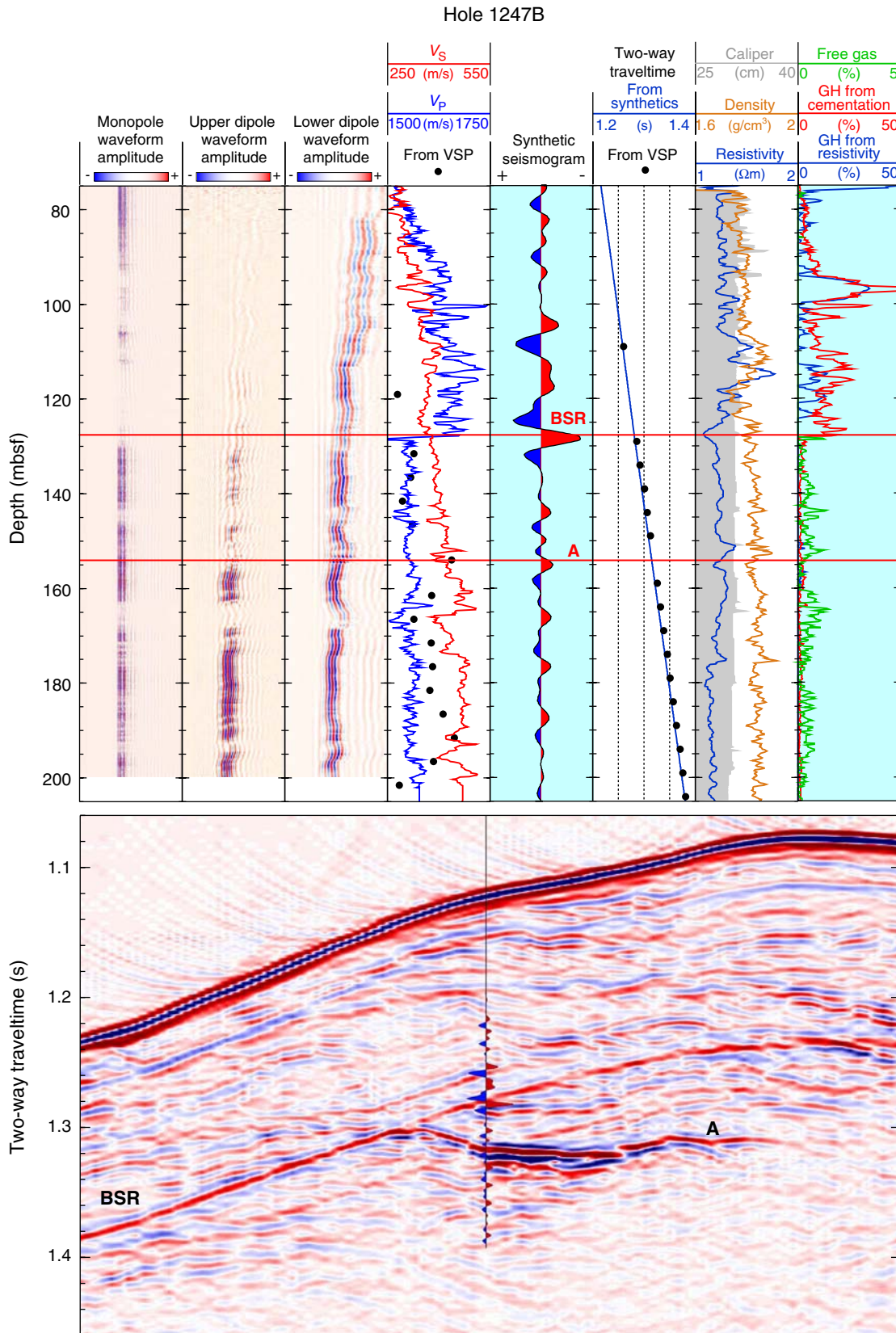
Figure F8. Results of the slowness-time coherence analysis of all the sonic logging waveforms recorded in Hole 1247B to derive the velocity logs. The colors indicate the coherence across the eight-receiver array corresponding to any velocity integrated over the entire time window. The black line indicates the final result. The gray dots indicate local maxima in coherence that could be interpreted as arrivals. BSR = bottom-simulating reflector, A = Horizon A.
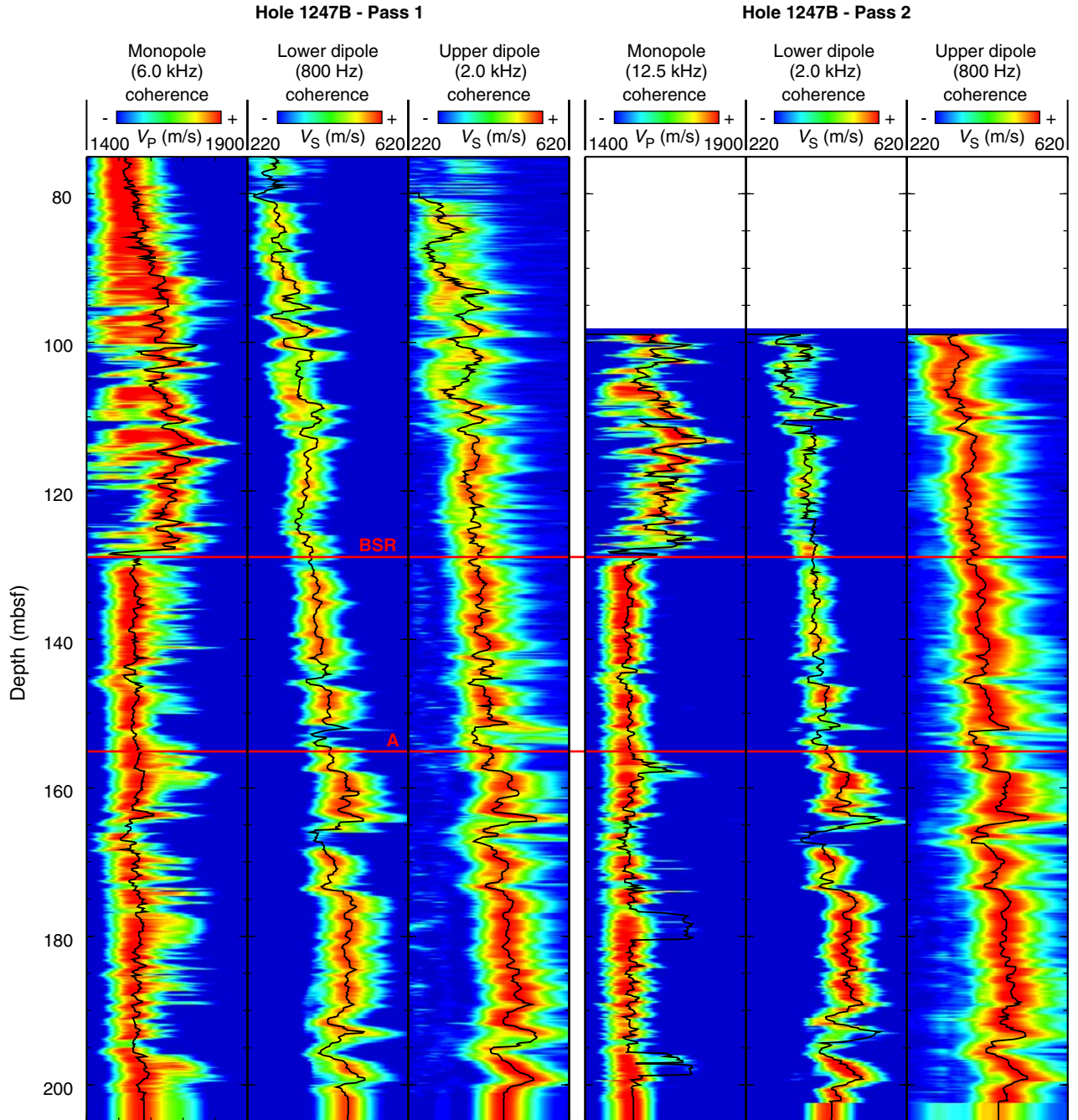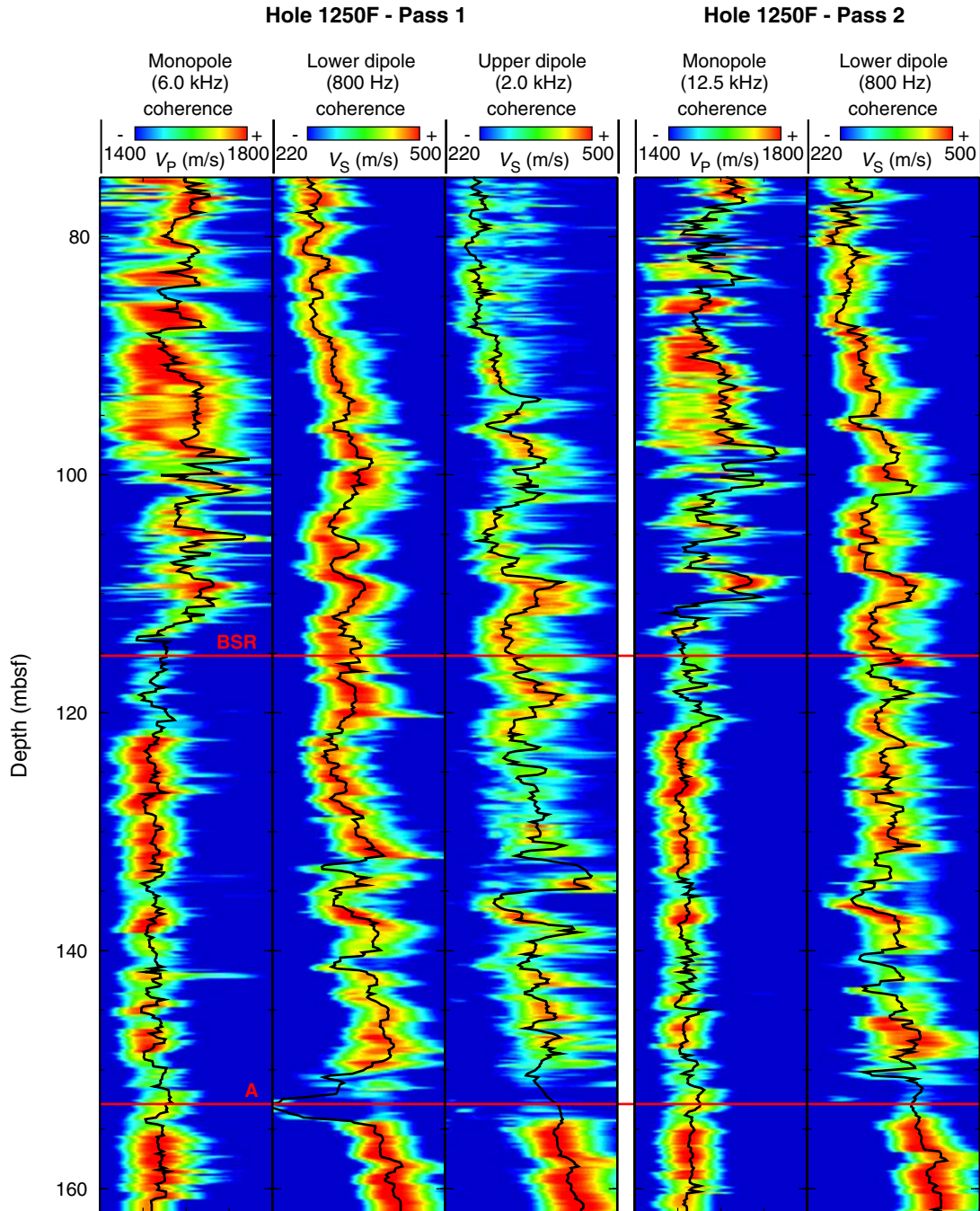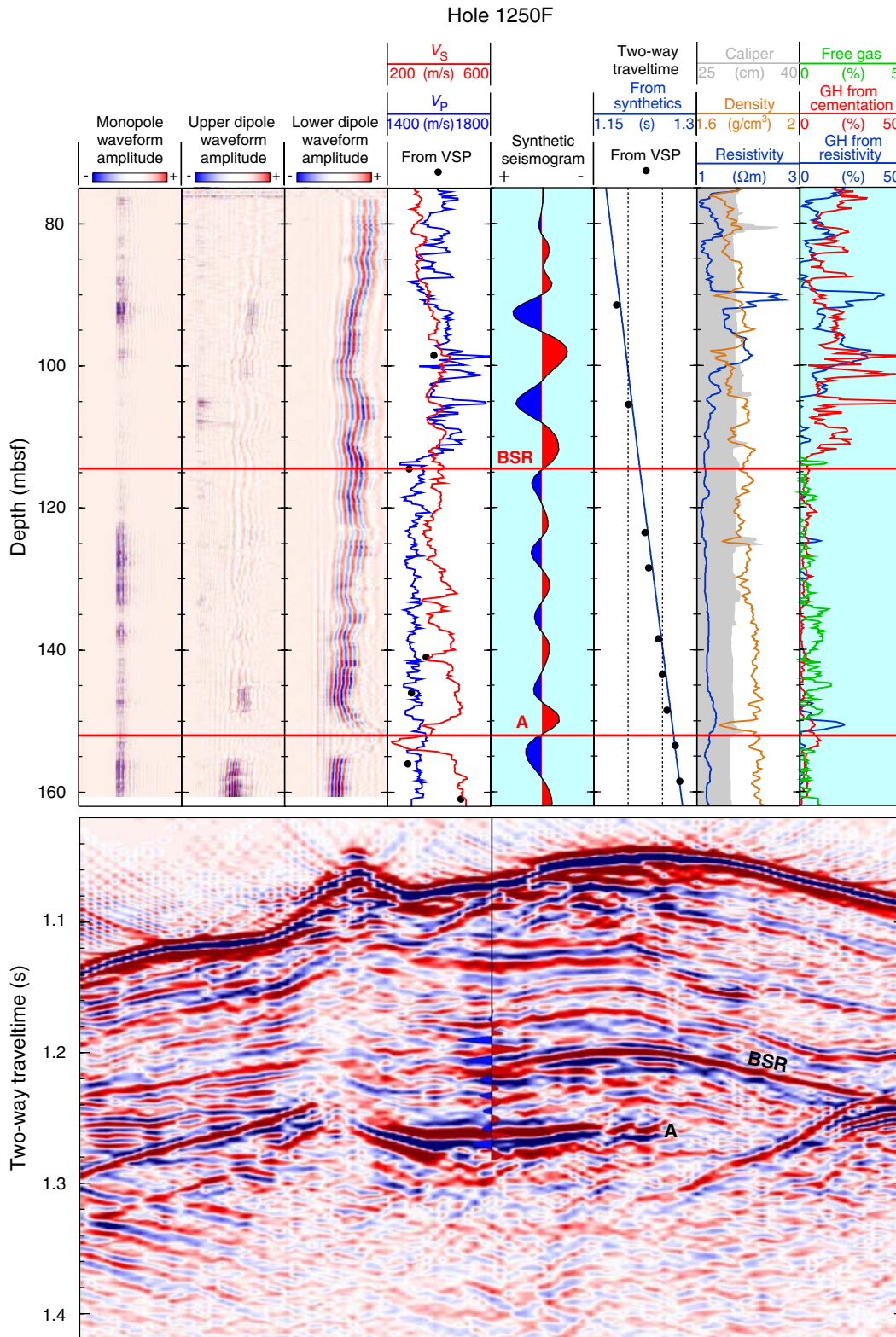
Figure F9. Wireline logs associated with the presence of gas hydrate (GH) in Hole 1247B. The synthetic seismogram and the gas hydrate concentration profiles were calculated from these logs. The velocity profile and time/depth relationship derived from the vertical seismic profile (VSP) (black dots) can be compared to the V_P log and to the time/depth relationship derived by correlation between the synthetic seismogram and the seismic data. The interval velocities calculated from the VSP have been smoothed by a five-sample moving average window. The synthetic seismogram is superimposed on a short east-west transect of the 3-D seismic survey for identification of the correlations. BSR = bottom-simulating reflector, A = Horizon A. (**Figure shown on next page.**)

Figure F9 (continued). (Caption shown on previous page.)

Figure F10. Results of the slowness-time coherence analysis of all the sonic logging waveforms recorded in Hole 1250F to derive the velocity logs. The colors indicate the coherence across the eight-receiver array corresponding to any velocity integrated over the entire time window. The black line indicates the final result. The gray dots indicate local maxima in coherence that could be interpreted as arrivals. BSR = bottom-simulating reflector, A = Horizon A.
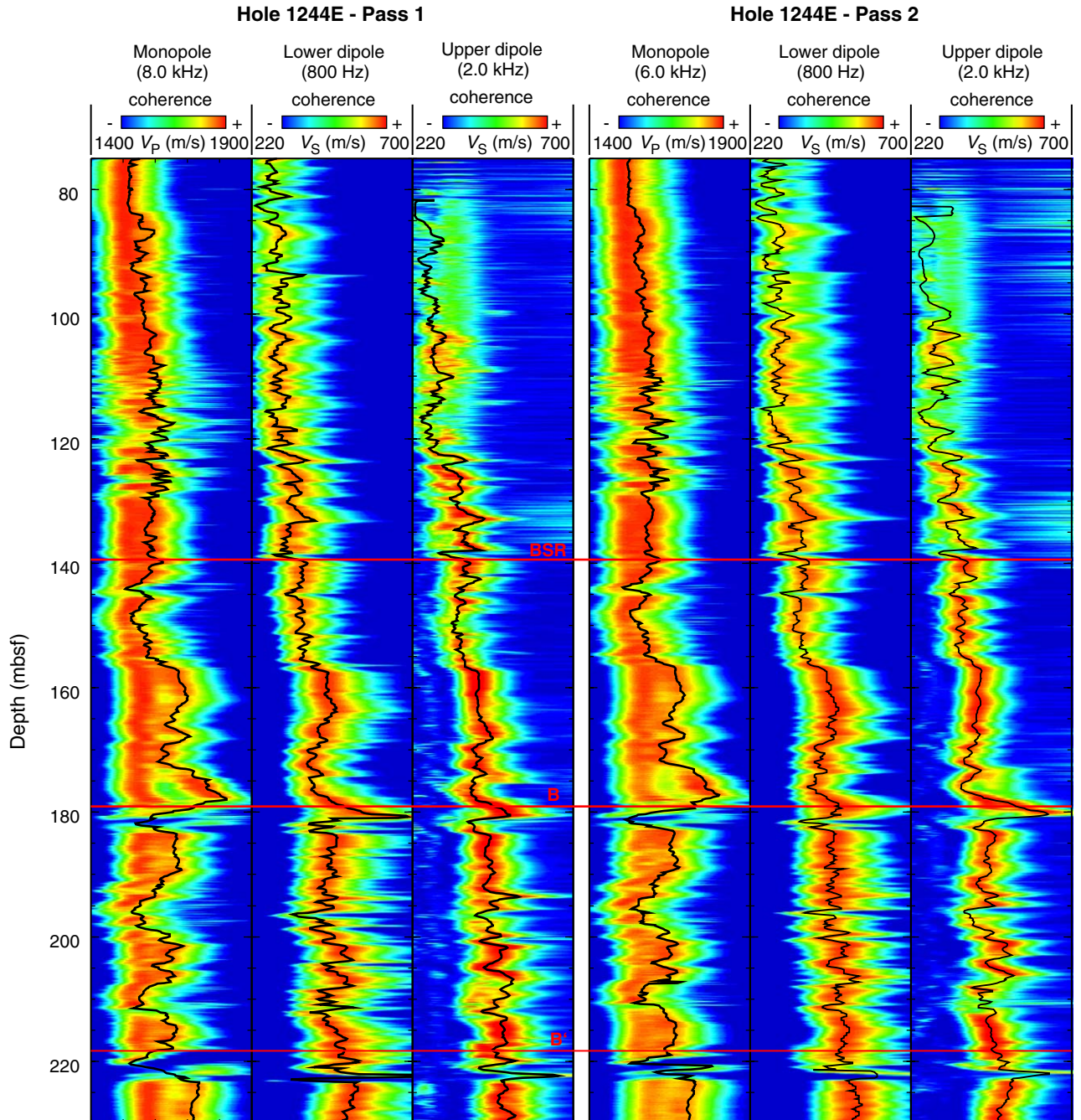
Figure F11. Wireline logs associated with the presence of gas hydrate (GH) in Hole 1250F. The synthetic seismogram and the gas hydrate concentration profiles were calculated from these logs. The velocity profile and time/depth relationship derived from the vertical seismic profile (VSP) can be compared to the V_P log and to the time/depth relationship derived by correlation between the synthetic seismogram and the seismic data. The synthetic seismogram is superimposed on a short east-west transect of the 3-D seismic survey for identification of the correlations. BSR = bottom-simulating reflector, A = Horizon A.

Figure F12. Results of the slowness-time coherence analysis of all the sonic logging waveforms recorded in Hole 1244E to derive the velocity logs. The colors indicate the coherence across the eight-receiver array corresponding to any velocity integrated over the entire time window. The black line indicates the final result. The gray dots indicate local maxima in coherence that could be interpreted as arrivals. BSR = bottom-simulating reflector, B = Horizon B, B′ = Horizon B′.

Figure F13. Wireline logs associated with the presence of gas hydrate (GH) in Hole 1244E. The synthetic seismogram and the gas hydrate concentration profiles were calculated from these logs. The velocity profile and time/depth relationship derived from the vertical seismic profile (VSP) (black dots) can be compared to the V_P log and to the time/depth relationship derived by correlation between the synthetic seismogram and the seismic data. The interval velocities calculated from the VSP have been smoothed by a five-sample moving average window. The synthetic seismogram is superimposed on a short east-west transect of the 3-D seismic survey for identification of the correlations. BSR = bottom-simulating reflector, B = Horizon B, B′ = Horizon B′. (**Figure shown on next page.**)

Figure F13 (continued). (Caption shown on previous page.)
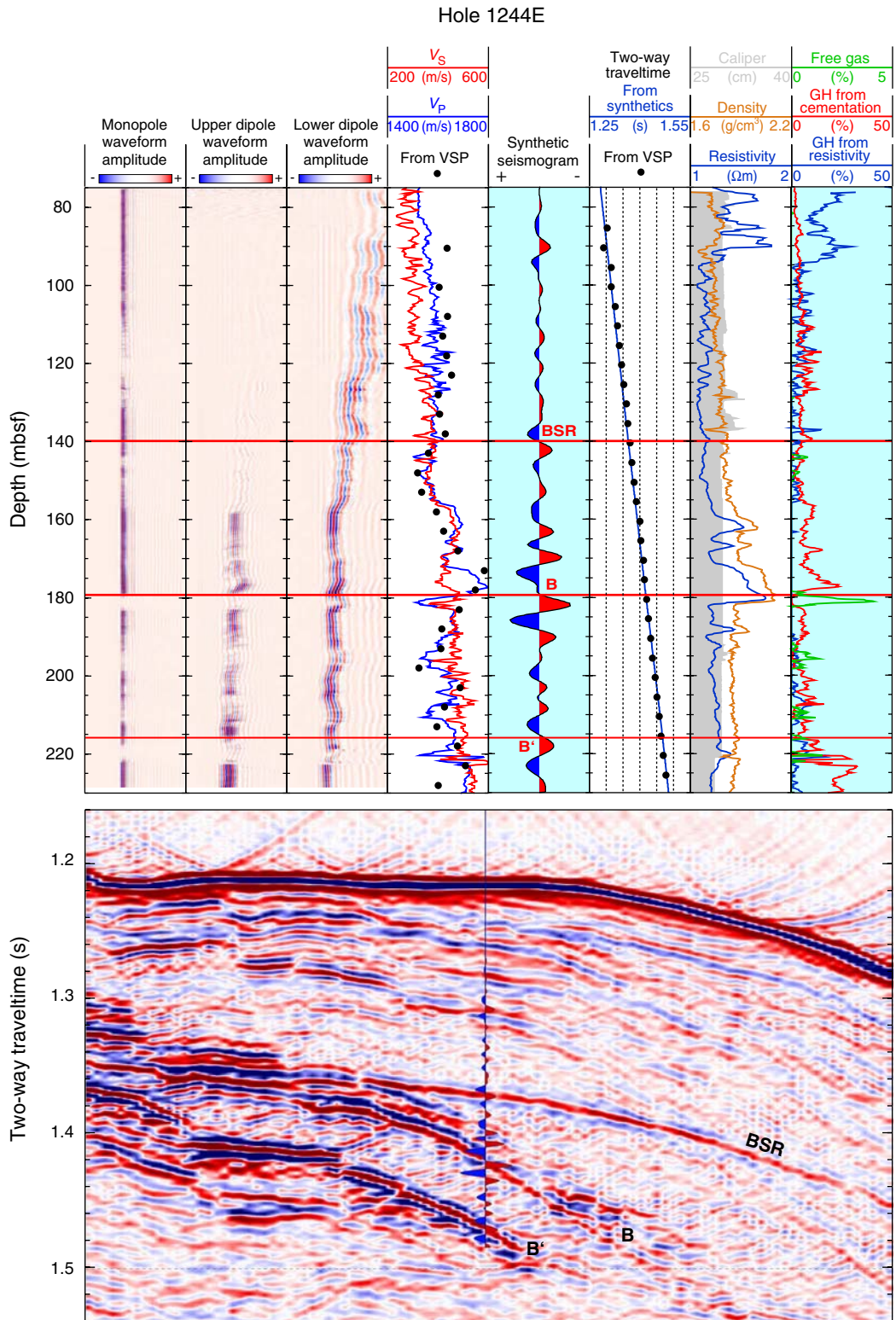

Hole 1244E

Figure F14. Results of the slowness-time coherence analysis of all the sonic logging waveforms recorded in Hole 1252A to derive the velocity logs. The colors indicate the coherence across the eight-receiver array corresponding to any velocity integrated over the entire time window. The black line indicates the final result. The gray dots indicate local maxima in coherence that could be interpreted as arrivals. BSR = bottom-simulating reflector.
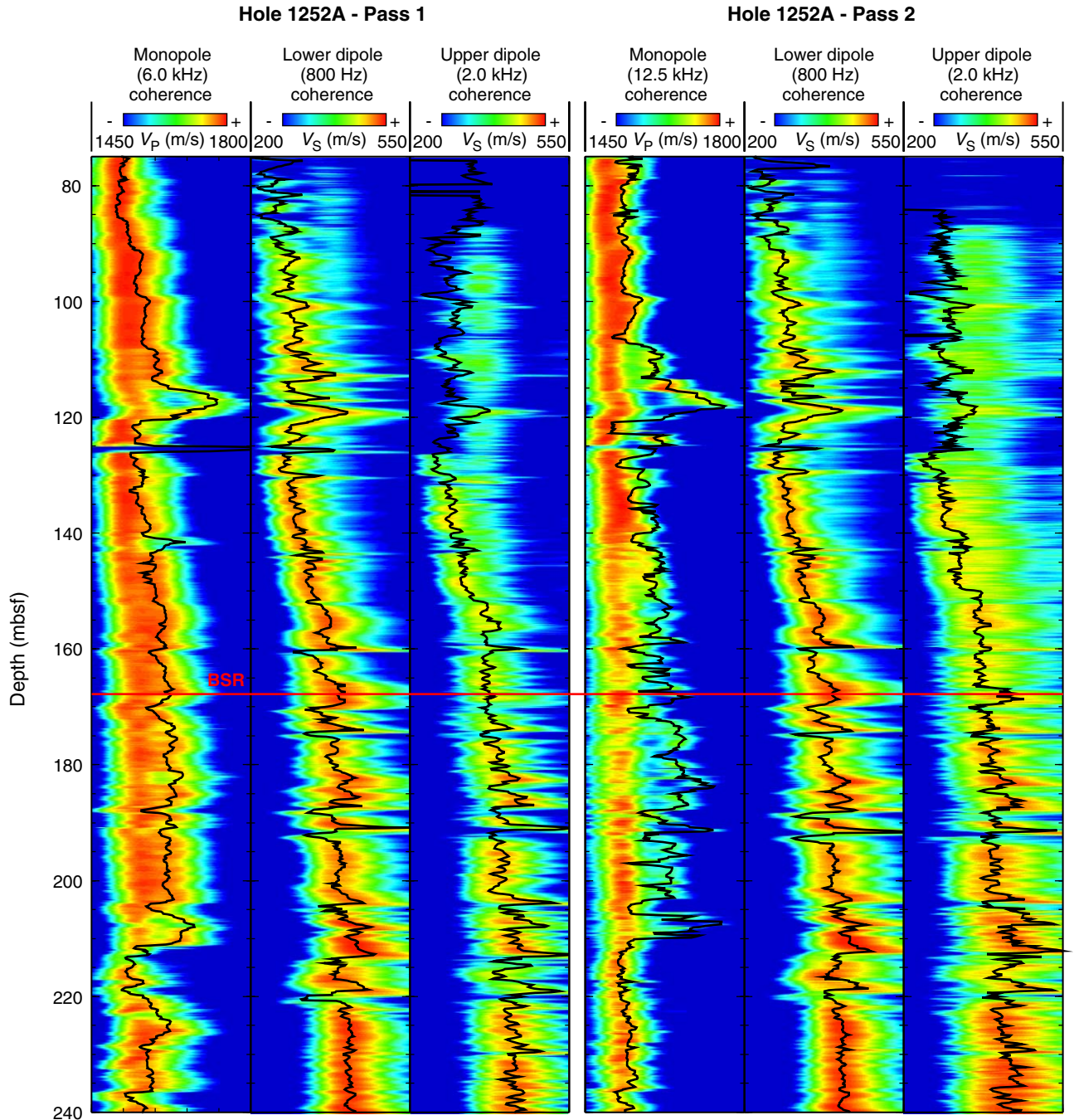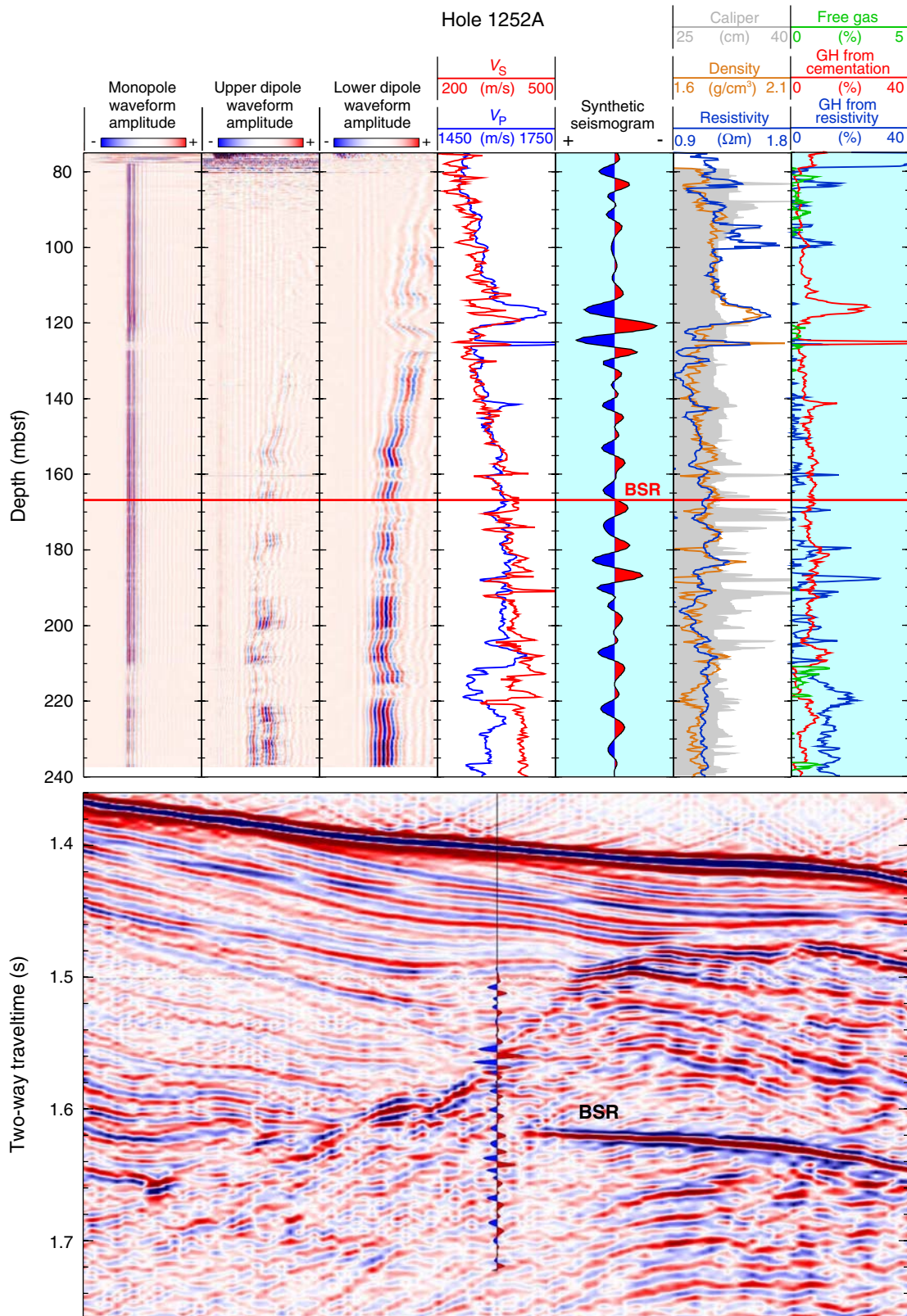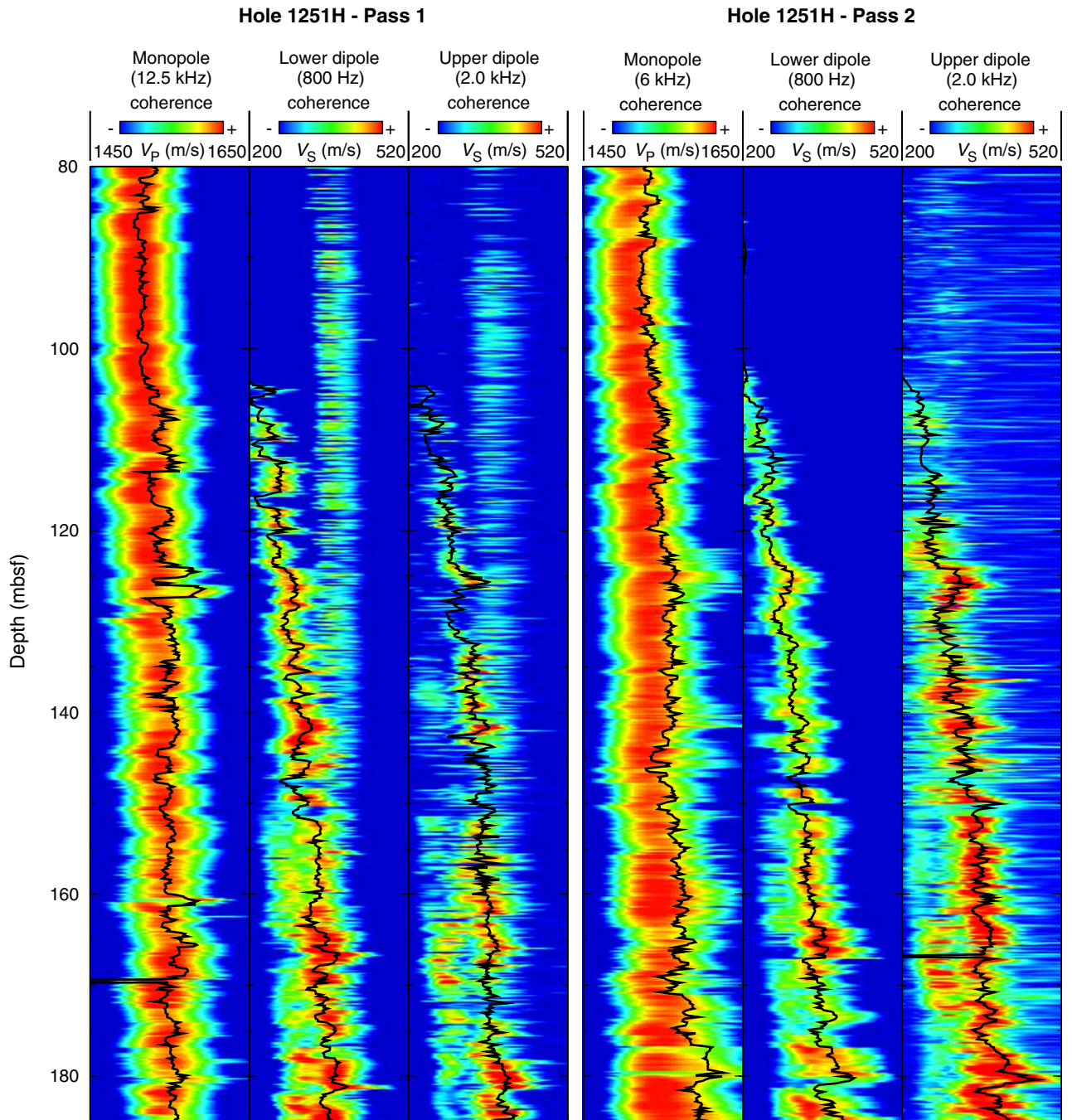
Figure F15. Wireline logs associated with the presence of gas hydrate (GH) in Hole 1252A. The synthetic seismogram and the gas hydrate concentration profiles were calculated from these logs. The synthetic seismogram is superimposed on a short east-west transect of the 3-D seismic survey for identification of the correlations. BSR = bottom-simulating reflector.

Figure F16. Results of the slowness-time coherence analysis of all the sonic logging waveforms recorded in Hole 1251H to derive the velocity logs. The colors indicate the coherence across the eight-receiver array corresponding to any velocity integrated over the entire time window. The black line indicates the final result. The gray dots indicate local maxima in coherence that could be interpreted as arrivals.

Figure F17. Wireline logs associated with the presence of gas hydrate (GH) in Hole 1251H. The synthetic seismogram and the gas hydrate concentration profiles were calculated from these logs. The time/depth relationship derived from the vertical seismic profile (VSP) can be compared to the time/depth relationship derived by correlation between the synthetic seismogram and the seismic data. The synthetic seismogram is superimposed on a short east-west transect of the 3-D seismic survey for identification of the correlations. BSR = bottom-simulating reflector. (**Figure shown on next page.**)

Figure F17 (continued). (Caption shown on previous page.)
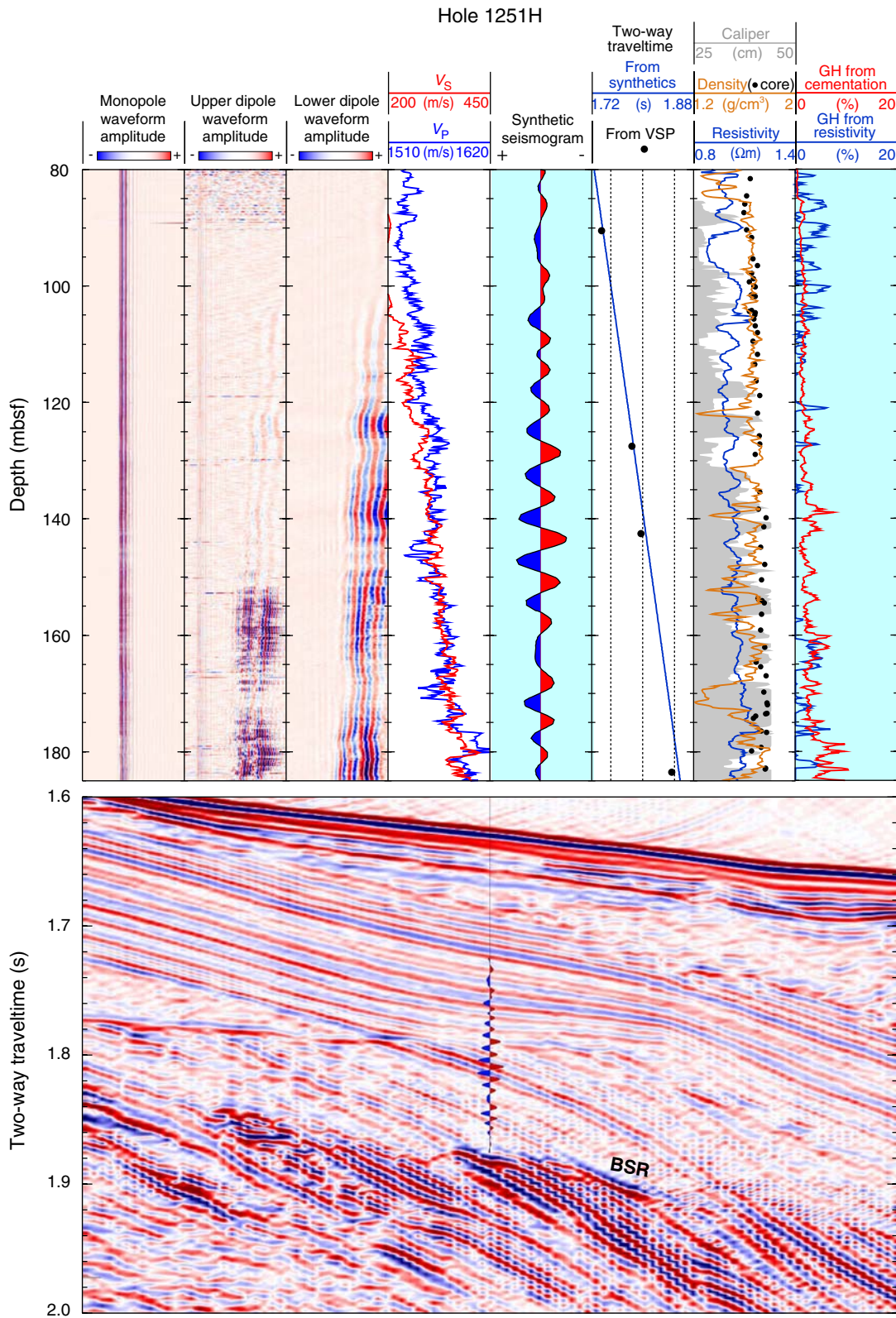
Table T1. Parameter used in the elastic models.

Parameter	Value
Number of contacts per grain (n)	9
Critical porosity (ϕ_c, %)	37
Grain density (kg/m^3)	2700
Water density (kg/m^3)	1000
Hydrate density (kg/m^3)	900
Sand bulk modulus ($K_{sand} \times 10^9$ Pa)	38
Sand shear modulus ($\mu_{sand} \times 10^9$ Pa)	44
Clay bulk modulus ($K_{clay} \times 10^9$ Pa)	21.2
Clay shear modulus ($\mu_{clay} \times 10^9$ Pa)	6.67
Pore water bulk modulus ($K_{water} \times 10^9$ Pa)	2.67
Hydrate bulk modulus ($K_h \times 10^9$ Pa)	7.9
Hydrate shear modulus ($\mu_h \times 10^9$ Pa)	3.3
Free gas bulk modulus ($K_{gas} \times 10^9$ Pa)	0.2